Lymphocyte-specific Protein Tyrosine Kinase Regulates Homologous Recombination (HR) DNA Repair and Targeting Enhances PARPi Utility in HR Proficient Ovarian Cancer

Goutam Dey[1+], Rashmi Bharti[1+], Chad Braley[1], Ravi Alluri[1], Emily Esakov[1], Katie Crean-Tate[2], Keith McCrae[1,5], Amy Joehlin-Price[3], Peter G. Rose[2], Justin Lathia[1,5], Zihua Gong[4,5], Ofer Reizes[1,5*]

1 Department of Cardiovascular and Metabolic Sciences, Lerner Research Institute, Cleveland Clinic Foundation, Cleveland, Ohio, USA
2 Division of Gynecologic Cancer, Women's Health Institute, Cleveland Clinic
3 Pathology and Lab Medicine, Cleveland Clinic
4 Cancer Biology, Lerner Research Institute, Cleveland Clinic
5 Case Comprehensive Cancer Center, Cleveland, OH

[+] co-first authors

* Address correspondence to:
Ofer Reizes, Ph.D.

Staff
Department of Cardiovascular and Metabolic Sciences
Lerner Research Institute
9500 Euclid Avenue
Cleveland Clinic
Cleveland, OH 44195
Email: reizeso@ccf.org
Direct: 216-445-0880

Running title: LCKi augments PARP targeted therapy in HR-proficient eEOC

Conflict of interest: Authors declare no conflict of interest.

Abstract

Poly-ADP Ribose Polymerase (PARP) inhibitors are clinically approved for the treatment of homologous recombination (HR) repair deficient tumors. PARP targeted therapy has limited efficacy in HR-proficient cancer. In this study, we identified the non-receptor lymphocyte-specific protein tyrosine kinase (LCK) as a novel regulator of HR repair pathways in endometrioid epithelial ovarian cancer (eEOC). Inhibition of LCK attenuates the expression of RAD51, BRCA1, and BRCA2 proteins necessary for HR-mediated DNA repair. HR repair in eEOC cells is LCK dependent. Upon DNA damage LCK expression is increased, and autophosphorylated, activated LCK is localized in the nucleus. LCK inhibition impairs RAD51 foci formation but augments γH2AX formation during DDR indicating reduced ability to repair DNA damage. DNA damage leads to direct interaction of LCK with RAD51 and BRCA1. Finally, attenuation of LCK sensitized HR-proficient eEOC cells to PARP inhibitor. Collectively, the findings identify a mechanism for expanding utility of PARP inhibitors.

Graphical Abstract

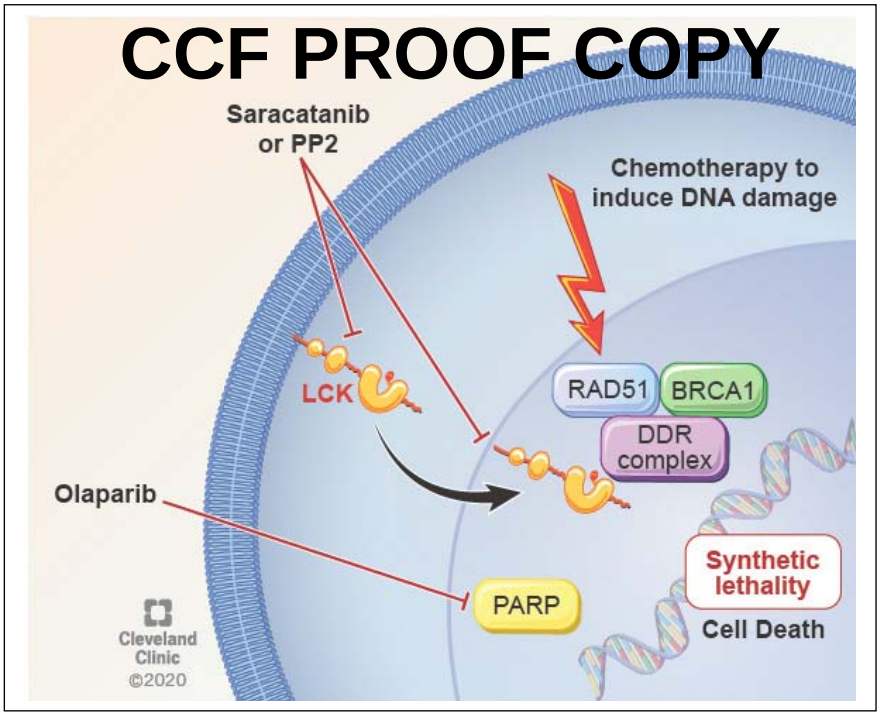

In Brief

Dey and colleagues identify the nonreceptor tyrosine kinase LCK as a mediator of homologous recombination directed DNA repair in ovarian cancer. The studies show that LCK inhibition (LCKi) is sufficient to augment Poly (ADP-Ribose) Polymerase inhibitor efficacy in Homologous Recombination (HR) proficient endometrioid ovarian cancer.

Highlights

- Nonreceptor tyrosine kinase LCK regulates expression of HR repair proteins RAD51, BRCA1 and BRCA2.
- LCKi induces HR deficiency in endometrioid epithelial ovarian cancer.
- DNA damage leads to autophosphorylation of LCK and co-immunoprecipitation with RAD51 and BRCA1.
- LCKi potentiates PARP targeted therapy in HR proficient ovarian cancer and expands the utility of the highly successful PARP inhibitors in the clinic.

Statement of significance

This study identifies a novel regulator and signaling pathway for maintaining HR repair during DNA damage. It further demonstrates a new opportunity to increase the utility of PARP inhibitors in HR-proficient eEOC cells.

Abbreviations: *eEOC: Endometrioid epithelial ovarian cancer*, *HR: Homologous recombination, LCK: Lymphocyte-specific protein tyrosine kinase, PARP: Poly ADP Ribose polymerase, DDR: DNA damage response, NHEJ: Non homologues end joining.*

Introduction

Epithelial ovarian cancer (EOC) is the second most common gynecologic malignancy in the United States, but the most common cause of gynecologic cancer death. It is estimated that 21,750 cases of EOC will be diagnosed and that 13,940 patients will die with EOC in the US in 2020 (1). Approximately 80% of endometrial cancers and 10% of ovarian cancers demonstrate endometrioid tumor histology (eEOC) (2). A small but clinically significant proportion of eEOC display high-grade histology, advanced stage (FIGO stage III-IV) and a poor 5-year survival of 6-24%, similar to that of the more aggressive high grade serous type of ovarian cancer (3). Moreover, somatic and germline mutation in HR genes occur in only a third of tumors, indicating the majority of eEOC are HR-proficient. Of note, eEOC shows a considerably higher rate of resistance to platinum-based chemotherapy (4) compared to serous carcinomas and does not commonly respond to targeted therapies such as Poly-(ADP-Ribose) Polymerase inhibitors (PARPi).

PARPi have emerged as new therapeutic options in the treatment of ovarian cancer (5-7) with recent studies showing prolonged median recurrence-free survival after primary therapy by more than 24 months (8). While the benefit of PARPi is greatest in BRCA1/2-mutated/deficient tumors, those with HR deficiencies also experience a benefit from this therapy (8). Conversely, PARPi and chemotherapy have so far shown limited efficacy in HR-proficient ovarian cancers. Further, platinum resistance is associated with HR-proficiency in EOC (9,10). This reduced efficacy of both platinum and PARPi therapy highlights an unmet clinical need in ovarian cancer patients.

Several strategies have been assessed to expand the utility of PARPi in HR-proficient cancers (5,11-13). RAD51, BRCA1 and BRCA2 are critical components of the HR repair complex. Studies have focused on disrupting this complex. Cyclin dependent kinase (CDK) proteins can regulate the HR repair pathway in a lung cancer model (14). Indeed, the CDK inhibitor, dinaciclib is able to attenuate the expression of RAD51 and BRCA proteins resulting in the inhibition of HR repair capacity and potentiation of the pharmacological effect of PARPi (12). However, there is no clinically approved drug for PARPi combination in HR-proficient cancers.

We previously determined that intracellular non-receptor tyrosine kinase, LCK regulates genes involved in DNA repair machinery in eEOC (15). We demonstrated the pharmacologic inhibition of LCK attenuated expression of homologous recombination DNA damage repair genes leading to sensitization of eEOC cells to cisplatin. In contrast, increased expression of LCK led to upregulation of DNA Damage Repair genes and increased resistance to cisplatin. As LCK modulates RAD51, BRCA1, and BRCA2 expression, we hypothesize that blocking LCK expression or inhibiting kinase activity sensitizes eEOC to PARPi. Here, we elucidate the mechanism of LCK in regulating HR DNA damage repair and a therapeutic approach to sensitize HR proficient eEOC to PARP inhibitors.

Results

LCK is sufficient to modulate HR repair protein expression in eEOC.

We tested whether LCK inhibition is sufficient to inhibit RAD51, BRCA1, and BRCA2 at the protein level. We focus on CP70 and SKOV3, both cisplatin resistant eEOC cells and considered HR proficient. CP70 and SKOV3 cells were transduced with lentivirus containing shRNA control (shCon) or LCK-targeted shRNA (LCK KD1, LCK KD4). Additionally, we generated LCK knock out (LCK KO) CP70 cells by CRISPR/Cas9. We confirmed silencing of LCK by immunoblotting followed by analysis of expression of BRCA1, BRCA2, and RAD51 by western blot analysis. In CP70 cells, we observed that LCK KD or KO attenuated protein expression of BRCA1, BRCA2 and RAD51 compared to shCon (Fig. 1A, and Supplementary Fig. S1A and C). Similarly, in SKOV3 cells, the protein expression of BRCA1, BRCA2 and RAD51 were attenuated in LCK knock down groups (Fig. 1A, and Supplementary Fig. S1B).

We next tested whether LCK overexpression would augment RAD51, BRCA1, and BRCA2 protein expression in eEOC. In contrast to LCK silencing, LCK overexpression led to induction of RAD51, BRCA1 and BRCA2 proteins in CP70 and SKOV3 cells (Fig. 1A, and Supplementary Fig. S1D and E). We further overexpressed LCK in CP70 LCK KO (C_LCK OE) background and observed a similar increase in expression of RAD51, BRCA1, and BRCA2 protein (Fig. 1A, and Supplementary Fig. S1F).

To test whether pharmacologic inhibition would attenuate DNA damage repair protein expression, we used PP2, a cell permeable small molecule inhibitor with LCK kinase

(17,18). We tested the efficacy of PP2 in CP70 and SKOV3 LCK OE cells. PP2 attenuated pLCK Y394, the autophosphorylation site of LCK in CP70 and SKOV3 LCK OE cells (Fig. 1B, and Supplementary Fig. S1G and H). γH2AX, a marker of DNA damage and replication stress was elevated by PP2 treatment indicative of either increased damage or reduced repair of DNA damage due to attenuation of BRCA1 and RAD51 by LCK inhibition. Notably, pY394 LCK inhibition also attenuates expression of RAD51, BRCA1, and BRCA2 in parental CP70 and SKOV3 as well as clear cell EOC, CRL1978 (Supplementary Fig. S2A).

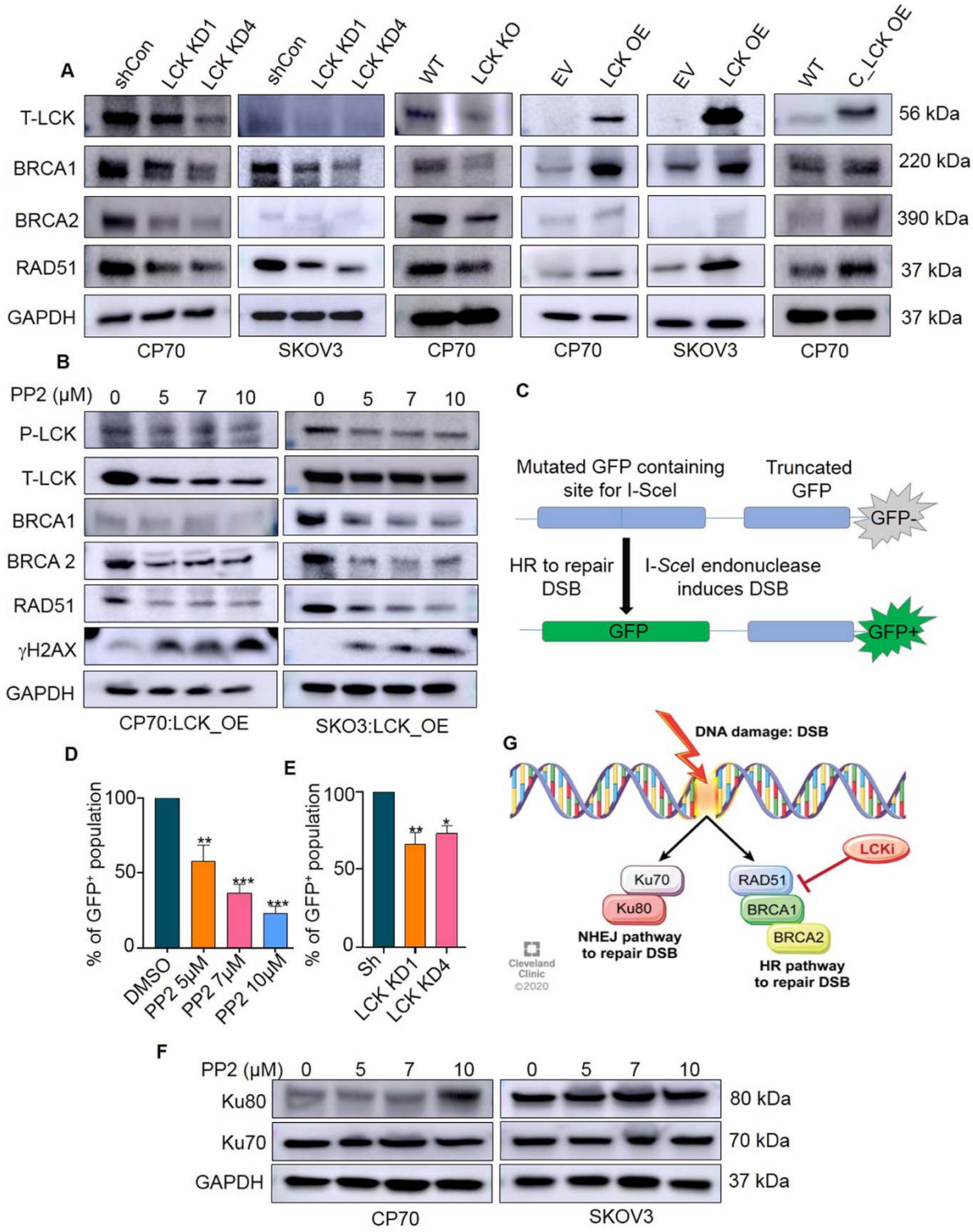

Fig 1: LCK modulates expression of HR repair proteins and LCK inhibition attenuates the HR repair pathway in eEOC cells. (A) Western blot analysis of CP70 and SKOV3 cells containing various lentiviral LCK KD, KO, OE and C_LCK OE (LCK overexpression in CRISPR/Cas9 background) to determine effects on LCK, BRCA1, BRCA2 and RAD51 expression. **(B)** Western blot analysis of CP70

and SKOV3 LCK OE cells treated with PP2 in a dose dependent manner for 48hrs, demonstrating the effects of a pharmacological inhibitor of LCK on. P-LCK, T-LCK, BRCA1, BRCA2, RAD51 and γH2AX protein expression. **(C)** Schematic of DNA repair assay in U2OS osteosarcoma cells stably transduced with the DR-GFP reporter system. This reporter system contains upstream gene-encoding mutated GFP, and downstream truncated GFP. Transfection of I-SceI endonuclease induces double strand breaks in the upstream gene. Following efficient HR repair, GFP expression is restored and can be utilized to indicate HR-efficient cells for quantification. **(D)** U2OS cells were treated with varying concentrations of the LCKi PP2 for 48h or **(E)** transfected with Sh Con, LCK KD1 or KD4 for 24h and incubated in serum enriched medium for another 24h. Cells were then subjected to DR-GFP assay. (**F**) CP70, and SKOV3 cells were treated with increasing concentrations of PP2 for 48h and cells were harvested, lysed, and immunoblotted for Ku70 and Ku80 protein expression. GAPDH was used as loading control. **(G)** Schematic model summarizing LCK inhibition specificity for HR DNA repair. (Unpaired t test, p*<0.05, p**<0.01, p***<0.001).

LCK inhibition attenuates HR DNA damage repair in eEOC.

To test whether LCK inhibition impairs HR-dependent DNA repair, we utilized the DR-GFP reporter assay to measure repair efficiency (25). The assay system is established in U2OS cells and provides a reporter for detection of cells capable of HR repair (Fig. 1C). U2OS cells with/without DR-GFP reporter system express endogenous LCK protein by western blot analysis (Supplementary Fig. S2B). PP2 treatment in a dose dependent manner led to significantly reduced GFP-positive population compared to DMSO-treated cells indicative of reduced DNA repair due to LCK inhibition (Fig. 1D). Likewise, shRNA silencing of LCK led to reduction in GFP positive population compared to shCon transduced cells (Fig. 1E). This indicates that LCK inhibition attenuates HR repair efficiency in cancer cells.

DNA damage leads to activation of several repair pathways including HR, and NHEJ (26). As our studies indicated LCK inhibition attenuates HR repair proteins, we assessed LCK impact on expression of alternative DNA repair pathways NHEJ in CP70 and SKOV3 (Fig. 1F). Ku80 and Ku70 proteins take part in NHEJ pathway (27). After PP2 treatment, Ku80 protein expression was elevated in CP70 cells. However, Ku80 was almost unchanged by PP2 treatment in SKOV3. Further, Ku70 protein expression was not changed in CP70 and SKOV3 after PP2 exposure. In parallel, Ku70 and Ku80 expression was not changed upon PP2 treatment in CRL1978 cells (Supplementary Fig. S2C). Collectively, the findings indicate LCK inhibition targets HR repair proteins independent of induction of NHEJ repair mechanisms (Fig. 2G)

DNA damage induces LCK dependent BRCA1 expression.

To determine whether DNA damage induces LCK expression and activation, we induced DNA damage in ovarian cancer cells using etoposide, ultraviolet radiation and methyl methanesulfonate (MMS). Dose dependent treatment of CP70 cells with etoposide or MMS led to increased LCK protein expression (Fig. 2A and Supplementary Fig. S3A and B). In SKOV3 cells, etoposide or MMS treatment led to increased phosphorylation of LCK at pY394 although total LCK protein remained unchanged (Supplementary Fig. S4A). Further, ultraviolet radiation treatment in CP70 cells was sufficient to increase LCK phosphorylation (Supplementary Fig. S4B). As expected, BRCA1and γH2AX expression was induced, indicative of increased DNA damage (Fig. 2A). Since DNA damage, particularly double strand breaks (DSB), and its repair machinery are mostly located in nucleus (28), we investigated whether DNA damage could induce the accumulation of LCK in the nucleus. High levels of LCK phosphorylation were detected in the nucleus of the cells treated with etoposide (Fig. 2B and Supplementary Fig. S3C). We observed that pLCK was nearly exclusively localized in the nucleus of etoposide-treated cells through cytoplasmic and nuclear fractionation followed by western blot. This is consistent with localization of pLCK by immunofluorescence (Fig. 2C). However, there was no detectable pLCK in the nucleus of DMSO-treated cells (Fig. 2C). Similar results were observed in SKOV3 cells (Supplementary Fig. S4C). We next tested whether inhibition of LCK would be sufficient to block BRCA1 expression in etoposide treated cells. Etoposide treatment in shCon cells showed increased BRCA1 protein expression, whereas treatment of LCK KD cells attenuated BRCA1 expression (Fig 2D and Supplementary Fig. S3D). We repeated these studies in CRISPR/CAS9 KO cells and observed attenuation of BRCA1 in LCK KO CP70 cells with no attenuation in parental cells (Fig. 2E and Supplementary Fig. S3E). These findings indicate that DNA damage induction of BRCA1 is disrupted by LCK inhibition.

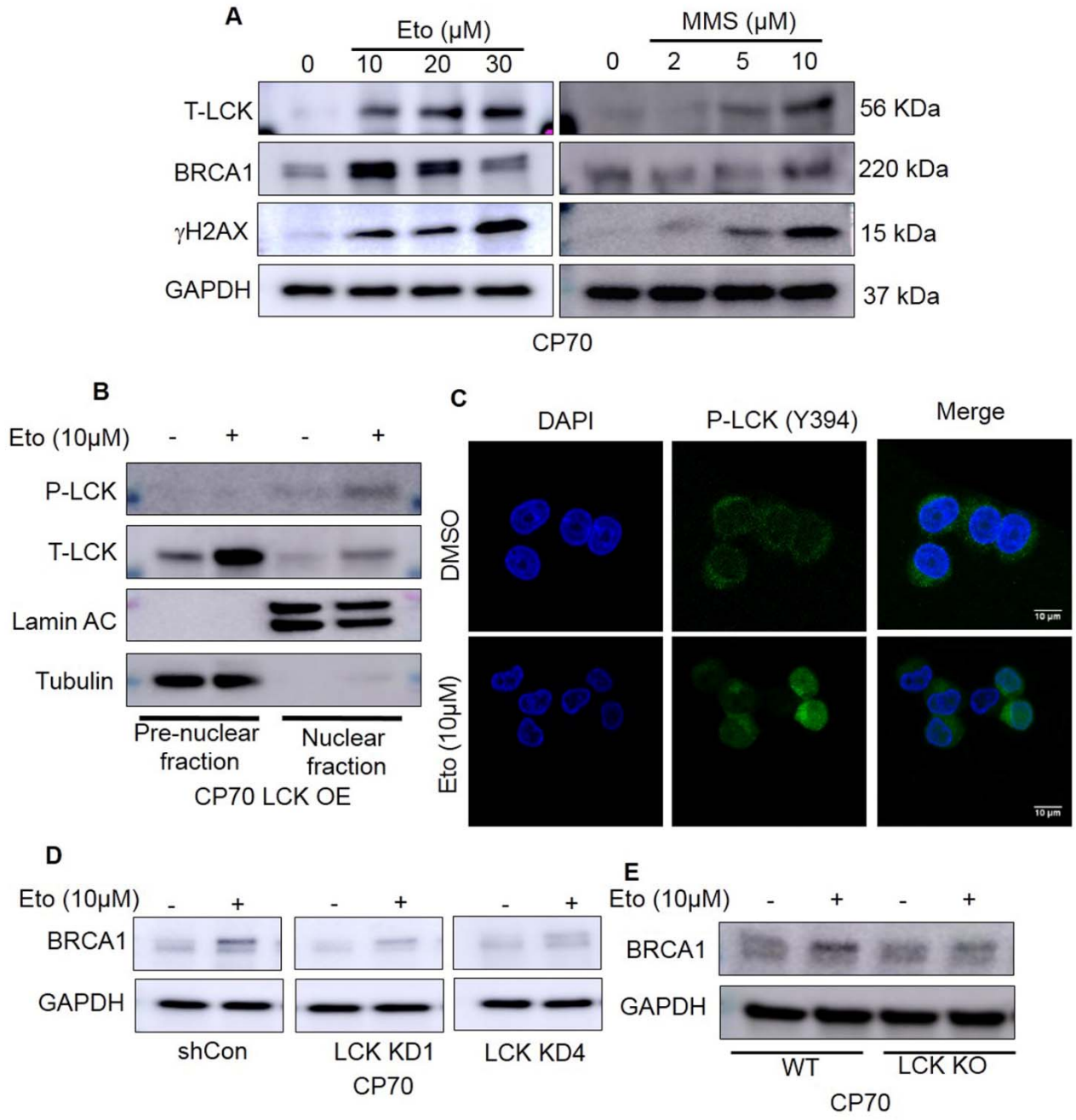

Fig 2: LCK is activated and LCK inhibition suppresses BRCA1 expression during DNA damage response. (A) Western blot analysis of T-LCK, BRCA1 and yH2AX expression following 24hrs etoposide or MMS treatment, followed by 24hrs recovery in CP70 cells. **(B)** Etoposide treated CP70 LCK OE cells were used for cytoplasmic and nuclear proteins extraction followed by western blot analysis. **(C)** Immunofluorescence study of etoposide treated CP70 cells. **(D)** Western blot analysis of etoposide/DMSO treated CP70 cells (Sh Con or LCK KD1 and KD4). **(E)** Western blot analysis of etoposide/DMSO treated CP70 cells (WT and LCK KO).

Repair of DNA double strand break is LCK dependent.

As γH2AX and RAD51 are markers of DNA damage and repair of DSB, we tested for foci formation in control and etoposide treated cells. LCK KO and C_LCK OE CP70 (LCK overexpression in CRISPR/Cas9-background) cells were treated with or without etoposide followed by immunofluorescence analysis to visualize γH2AX foci (Fig. 3A, B and Supplementary Fig. S5A). In the absence of etoposide, γH2AX foci formation was not detected. However, γH2AX foci formation was increased in naïve CP70 (WT) cells treated with etoposide. γH2AX was significantly increased in LCK KO cells treated with etoposide, but was nearly completely blocked by C_LCK OE (Fig. 3A and B).

In parallel, we assessed RAD51 foci formation in LCK KO and C_LCK OE CP70 cells treated in the absence or presence of etoposide (Fig. 3C, D and Supplementary Fig. S5B). As with γH2AX, no RAD51 foci were observed in WT, LCK KO, and C_LCK OE cells treated with DMSO. In contrast, etoposide treatment led to a significant increase in RAD51 foci in naive CP70 cells that was significantly suppressed in LCK KO cells (Fig. 3C, D and Supplementary Fig. S5B). Further, RAD51 foci formation was significantly increased in C_LCK OE cells treated with etoposide. This data supports the conclusion that LCK can regulate HR repair during DNA damage response (DDR).

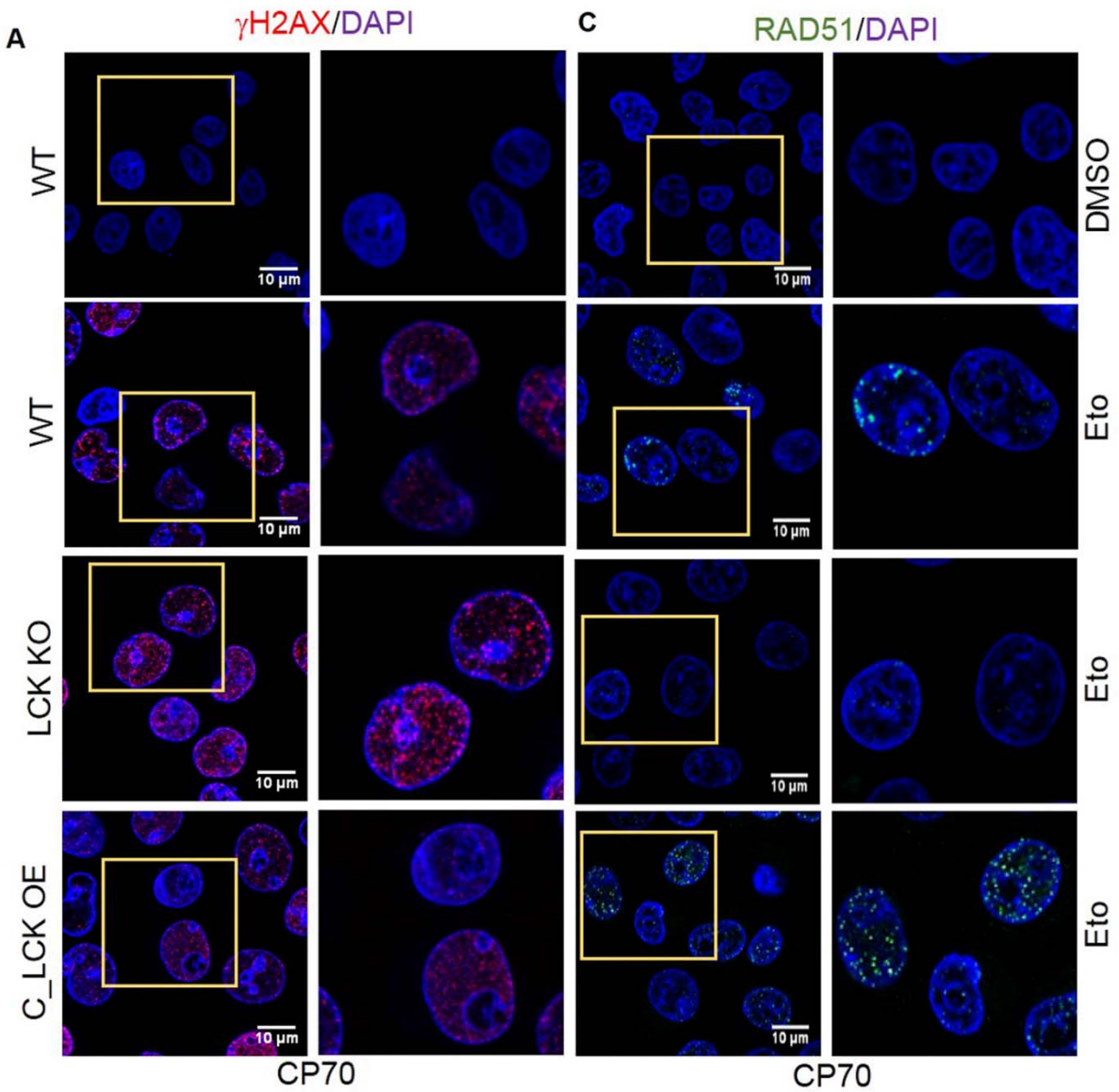

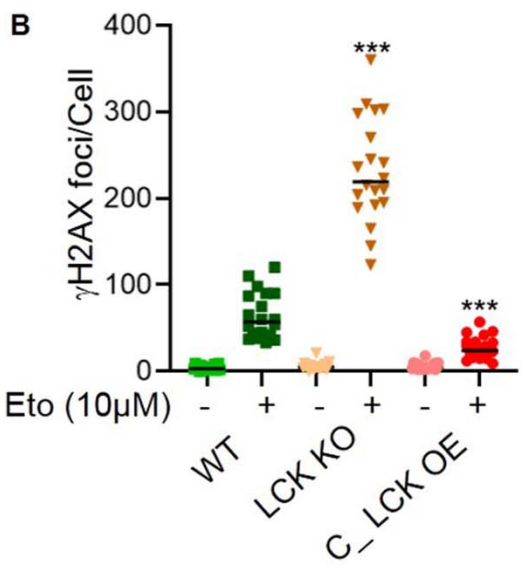

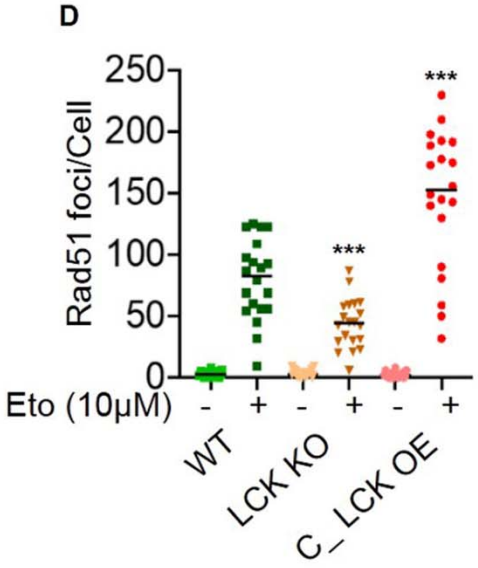

Fig 3: LCK regulates DNA damage and repair. (A and B) CP70 WT, LCK KO (CRISPR/Cas9) and LCK OE (In CRISPR background) cells were treated with DMSO/etoposide 10μM for 24h. Then cells were kept in drug-free media for another 24h. Then immunofluorescence study was performed to visualize γH2AX foci formation in different groups. Scale bar represents 10μm. γH2AX foci was counted by image J software and 20 cells were counted to plot in the graph. **(C and D)** CP70 WT, LCK KO (CRISPR/Cas9) and LCK OE (In CRISPR background) cells were treated with DMSO/etoposide 10μM for 24h. Cells were put in drug free media for another 24h. Then immunofluorescence study was performed to visualize RAD51 foci formation in different groups. RAD51 foci in 20 cells were counted by image J software. Level of significance is shown by estimating the p values (p*<0.05, p**<0.01, p***<0.001) by Graph pad Prism software.

LCK complexes with RAD51 and BRCA1 in response to DNA damage.

As pLCK is localized in the nucleus in response to DNA damage and can induce BRCA1 and RAD51, we tested whether LCK directly interacts with RAD51 and BRCA1 in nuclear extracts. CP70 and SKOV3 cells were transduced with a myc-tagged LCK (Fig. 4A and Supplementary Fig. S6). We treated cells in the absence or presence of etoposide, isolated nuclei, and performed an IP with myc antibodies. Neither BRCA1 nor RAD51 were detected in untreated cells. In contrast, CP70 and SKOV3 treated with etoposide showed expression of Myc-LCK, RAD51, and BRCA1 (Fig. 4B and C). Importantly, we were able to show RAD51 co-immunoprecipitated with LCK from etoposide treated LCK overexpressing SKOV3 cells. LCK and BRCA1 are detected in RAD51 immunoprecipitates (Fig. 4D). These findings indicate that in response to DNA damage, LCK interacts with a complex containing RAD51 and BRCA1 (Fig. 4E).

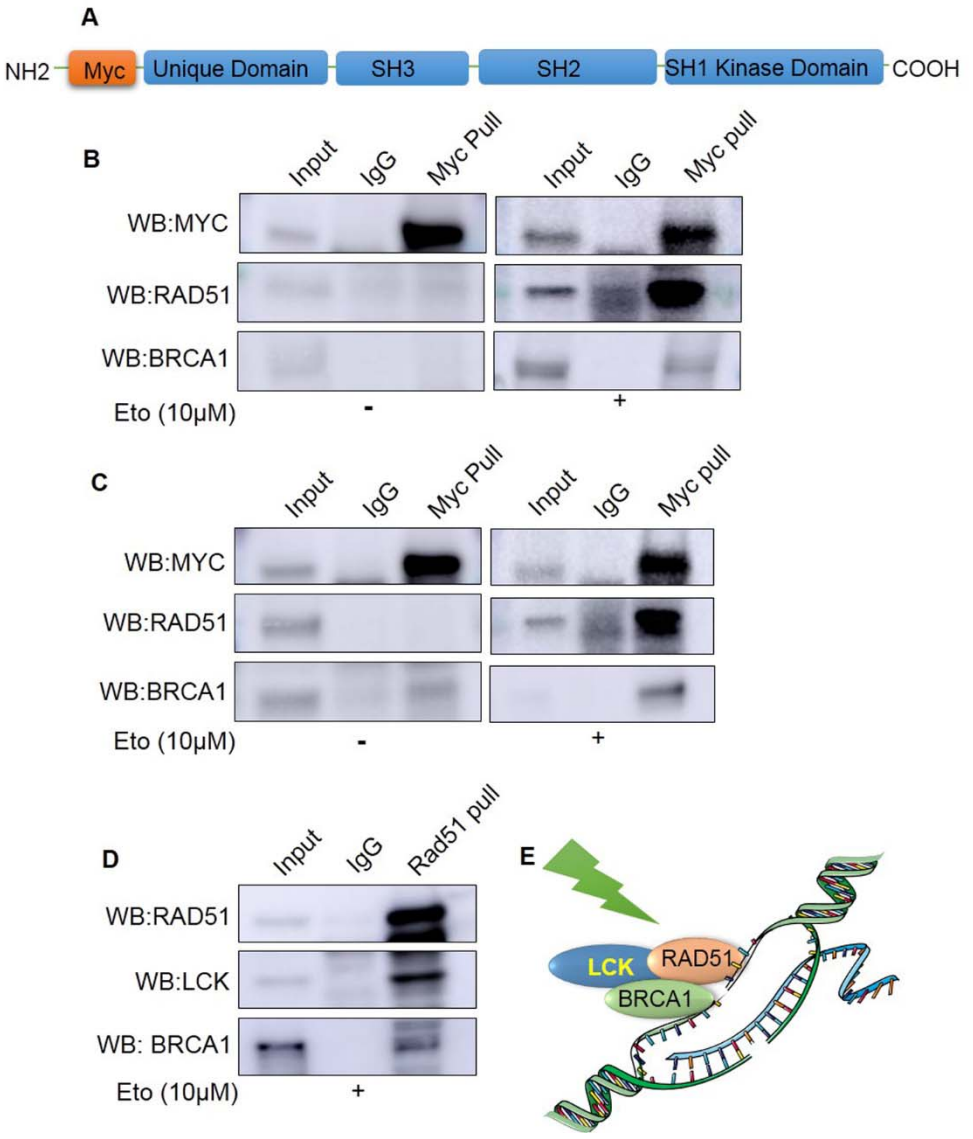

Fig 4: LCK interacts with RAD51 and BRCA1 during DNA damage response. (A) Schematic of Myc tagged LCK construct. **(B)** Myc tagged LCK expressing CP70 cells were treated with vehicle (DMSO) or etoposide. Cells were harvested, lysed, and nuclei were purified. Immunoprecipitation with Myc followed by immunoblotting for Myc, BRCA1, and RAD51. **(C)** Myc tagged LCK expressing SKOV3 cells were treated with vehicle or etoposide. Myc protein was pull down to determine the interaction of LCK with RAD51 and BRCA1 by co-immunoprecipitation study. **(D)** LCK overexpressing SKOV3 cells were treated with etoposide. RAD51 was pulled down from protein lysate. Then the expression of LCK and RAD51 was checked in pulled down protein sample by co-immunoprecipitation study. **(E)** Schematic of LCK binding partners during DNA damage response.

LCK kinase activity is essential for HR repair.

LCK interacts with BRCA1 and RAD51 in response to DNA damage and here we tested whether kinase activity and autophosphorylation are necessary for activity and DNA repair. We generated LCK mutants K273R, Y192F, and Y394F and transduced into LCK KO CP70 cells (Fig. 5A). For full activation of LCK kinase, presence of tyrosine at

position 394 and lysine at position 273 is essential for autophosphorylation, conformational change and phosphate group transfer (29). Further phosphorylation at Y192 inhibits the function of LCK and leads to negative regulation (30). Thus, C_ LCK OE and C_ LCK Y192F mutant retain kinase activity while C_ LCK K273R and C_ LCK Y394F mutants lose kinase activity. We performed IP studies in etoposide treated cells and determined that OE, and C_ LCK Y192F were able to coIP BRCA1 and RAD51, whereas C_ LCK K273R and C_ LCK Y394F did not co-immunoprecipitate (co-IP) BRCA1 and RAD51 (Fig 5B). We next tested for γH2AX and RAD51 foci formation in the C_ LCK OE, C_ LCK K273R, C_ LCK Y192F, and C_ LCK Y394F transduced cells. As expected, C_ LCK OE and C_ LCK Y192F exhibited similar level of foci formation in response to etoposide (Fig. 5C, D and E). C_ LCK K273R and C_ LCK Y394F showed increased γH2AX foci and reduced RAD51 foci in etoposide treated cells (Fig. 5C, D, E and Supplementary Fig. S7A, B). We performed a timed experiment with etoposide treated CP70 cells and determined that at time 0h, the extent of γH2AX foci were lowest in the C_ LCK OE and C_ LCK Y192F cells compared to WT cells. Moreover, KO, C_ LCK Y394F, and C_ LCK K273R cells exhibited greatest γH2AX foci formation at any time point (Supplemental Fig. 7C, D). We further assayed the cells for etoposide sensitivity. We determined that naïve CP70 cells exhibited an IC_{50} of 5μM to etoposide. C_ LCK OE and C_ LCK Y192F exhibited increased resistance to etoposide, whereas C_ LCK K273R and C_ LCK Y394F showed increased sensitivity to etoposide (Fig. 5F and G). These findings lead to the hypothesis that LCK inhibition would sensitize cells to PARPi.

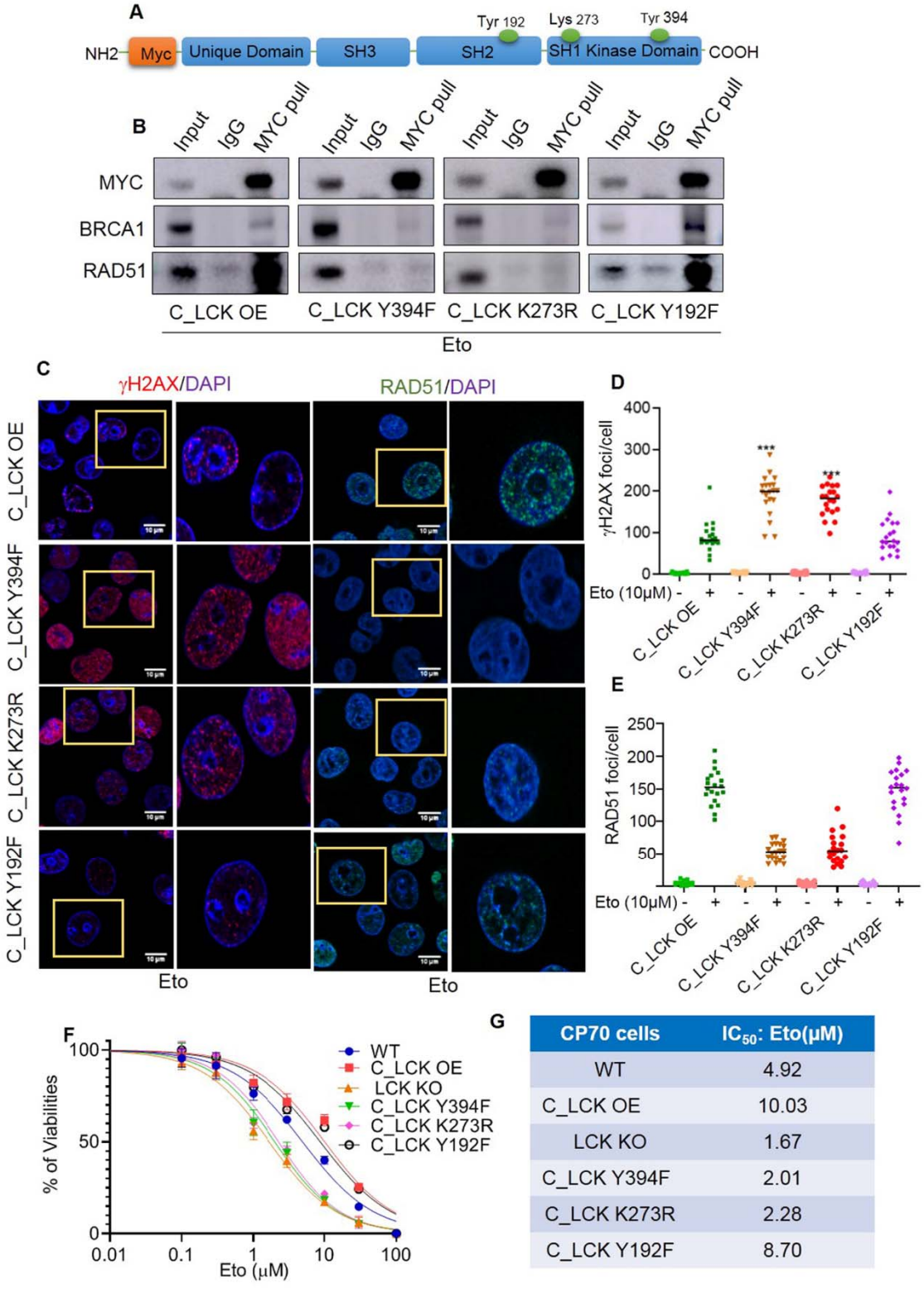

CP70 cells	IC_{50}: Eto(μM)
WT	4.92
C_LCK OE	10.03
LCK KO	1.67
C_LCK Y394F	2.01
C_LCK K273R	2.28
C_LCK Y192F	8.70

Fig 5: LCK kinase activity is essential for HR repair. (A) Structure of MYC labelled LCK construct. LCK Y394F, LCK K273R, LCK Y192F mutants were generated by site directed mutagenesis. These mutants were further introduced in CP70 cells having CRISPR background. **(B)** CP70 cells (MYC tagged LCK, LCK Y394F, LCK K273R, and LCK Y192F) were treated with etoposide/DMSO for 24h. Then cells

were put in drug free media for 24h. Cells were collected and nuclear proteins were isolated. MYC antibodies were used for co-immunoprecipitation study to visualize the complex formation with RAD51 and BRCA1 proteins. **(C)** CP70 cells (LCK OE, LCK Y394F, LCK K273R, and LCK Y192F) were treated with etoposide for 24h**.** Cells were then kept in drug-free media for 24h. Immunofluorescence was performed to visualize γH2AX and RAD51 foci formation. **(D, E)** Quantification of γH2AX and RAD51 foci formation in CP70 cells by Image J software. **(F)** CP70 cells (WT, LCK OE, LCK KO, LCK Y394F, LCK K273R, and LCK Y192F) were treated with etoposide in a dose dependent manner for 48h. Then cell titer glow viability assay was performed to check cell viability. **(G)**The table shows IC_{50} values of etoposide in CP70 cells. Level of significance is shown by estimating the p values (p*<0.05, p**<0.01, p***<0.001) by Graph pad Prism software.

LCK inhibition augments PARPi induced DNA damage and genomic instability.

We performed single cell gel electrophoresis (alkaline COMET) assay to quantify the extent of double and single strand DNA breaks by visualizing tail area (31). CP70 and SKOV3 cells were incubated with PP2, Olaparib, and their combination. Treated cells were processed and stained with SYBR gold to detect and measure the tail moment (Fig. 6A). PP2 and Olaparib displayed a comparable increase in comet tails compared to DMSO (Fig. 6B). The combination of PP2 and Olaparib induced a fourfold increase in comet tail area compared to monotherapy with PP2 or Olaparib (Fig. 6B).

PARP inhibitors are reported to induce genomic instability leading to chromosomal aberration and DNA damage in cancer cells (23,32). Chromosomal damage can be detected by chromosomal breaks, gaps, and radial formations. We identified multiple breaks, gaps, and radial formation in PP2 and Olaparib treated cells (Fig. 6C). PP2 and Olaparib displayed a comparable increase in chromosomal damage compared to DMSO (Fig. 6D). The combination of PP2 and Olaparib displayed increased chromosomal damage in both CP70 and SKOV3 cells (Fig. 6D).

Based on this analysis, we assessed whether the LCKi PP2 could synergize with PARPi Olaparib to augment DNA damage response (Fig. 6E). Olaparib treatment leads to increased BRCA1 and small increase in γH2AX expression (Fig. 6E). Co-treatment of cells with PP2 is sufficient to suppress BRCA1 expression and significantly augment γH2AX expression in a dose-dependent manner (Fig. 6E). Collectively, these findings indicate LCK inhibition is sufficient to sensitize eEOC to PARPi.

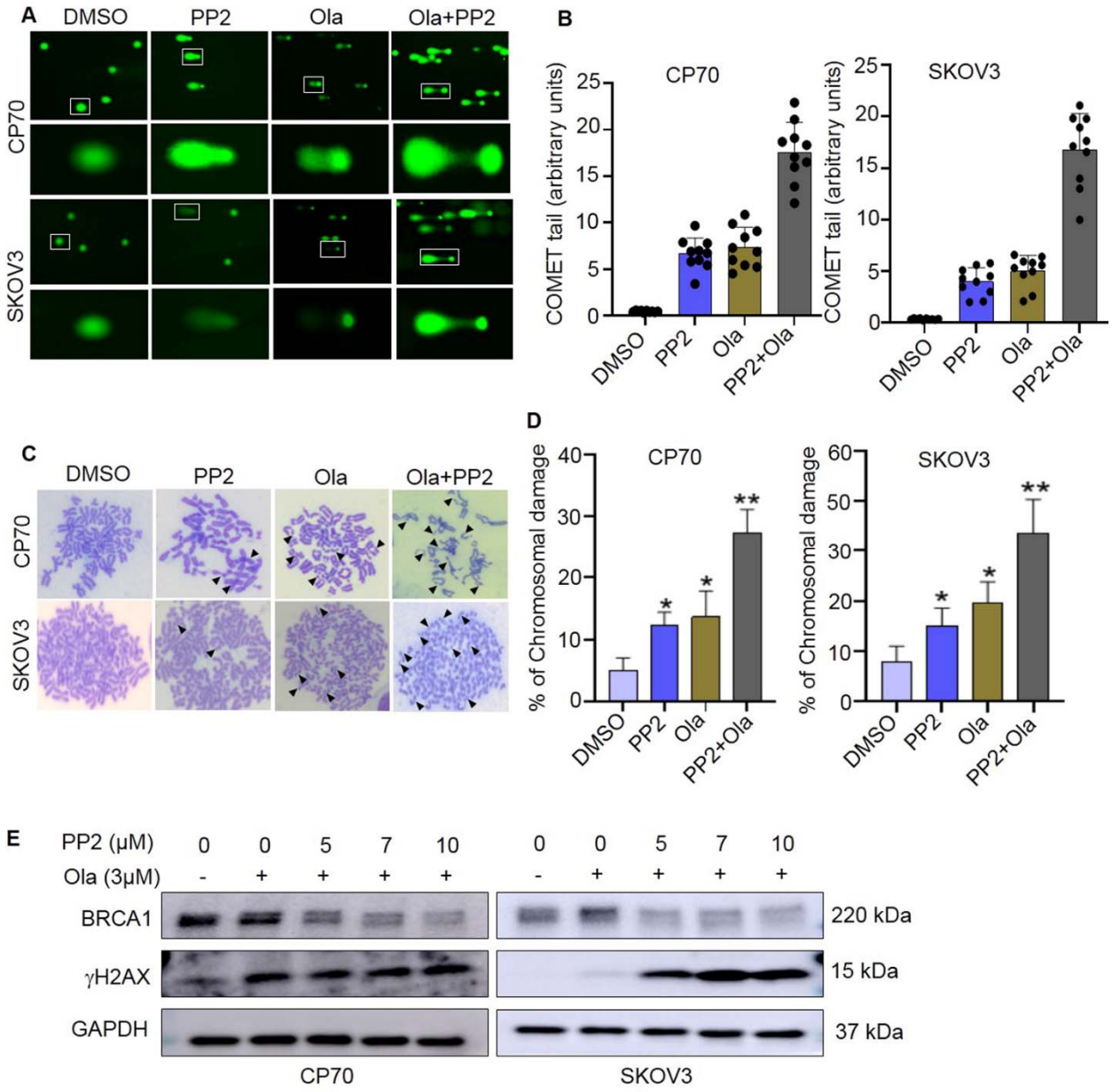

Fig 6: LCKi promotes genomic instability and augments PARPi induced genomic instability in ovarian cancer cells. **(A)** Single cell electrophoresis or COMET assay was used to validate and independently quantify the observed DNA damages. CP70 and SKOV3 cells were treated with PP2 5μM and/or Olaparib 3μM for 48h. Cells (1×10^5 Cells/ml) were then collected and mixed with LMAgarose (1:10 V/V). Then, 50L of LMAgarose solution was put on COMET slide and subjected to single-cell gel electrophoresis. **(B)** Extent of DNA damage was estimated based on measurement of COMET tail area using Image J. **(C)** CP70 and SKOV3 cells treated with PP2 5μM and/or Olaparib 3μM for 48h then had the chromosomal aberration assay performed. The arrow indicates the presence of abnormalities in chromosomes including breaks, gaps, and radials. **(D)** Abnormities in chromosomes were quantified (Chromosomal break, gap, radial formation) by counting by visual observation. **(E)** CP70 and SKOV3 cells were treated with Olaparib and PP2 for 48h. Cells were harvested, lysed, and blotted for BRCA1 and γH2AX. Level of significance is shown by estimating the p values (p*<0.05, p**<0.01, p***<0.001) by Graph pad Prism software.

LCK inhibition potentiates therapeutic efficacy of PARPi in cell culture.

Our findings indicate LCK inhibition leads to HR deficiency. As proof of concept, we tested the efficacy of LCK silencing to increase sensitivity to Olaparib in SKOV3 and CP70 cancer cells based on colony formation assay. Olaparib sensitivity was analyzed in parental (WT), LCK KO, LCK OE, as well as LCK mutants Y394F, K273R, and Y192F on LCK KO background CP70 cells (Fig. 7A). We quantified the colony formation and determined that sensitivity of CP70 to Olaparib is high in LCK KO, LCK Y394F and LCK K273R compared to WT CP70 cells (Fig. 7B and C). Further, sensitivity of CP70 to Olaparib is reduced in LCK OE and LCK Y192F cells. We replicated the findings in shRNA KD CP70 and SKOV3 cells (Supplementary Fig. S8A and B). shCon, LCK KD1 and LCK KD4 cells were treated with increasing concentrations of PARPi, Olaparib and plated for colony formation. In CP70 cells, LCK silencing inhibited colony formation more efficiently in Olaparib treated cancer cells compared to shCon treated cells (Supplementary Fig. S8). Similarly, in SKOV3 cells, the number of colonies were significantly decreased after Olaparib treatment in LCK KD1 and LCK KD4 cells compared to shCon cells. These findings demonstrated that Olaparib is more effective in LCK deficient cancer cells.

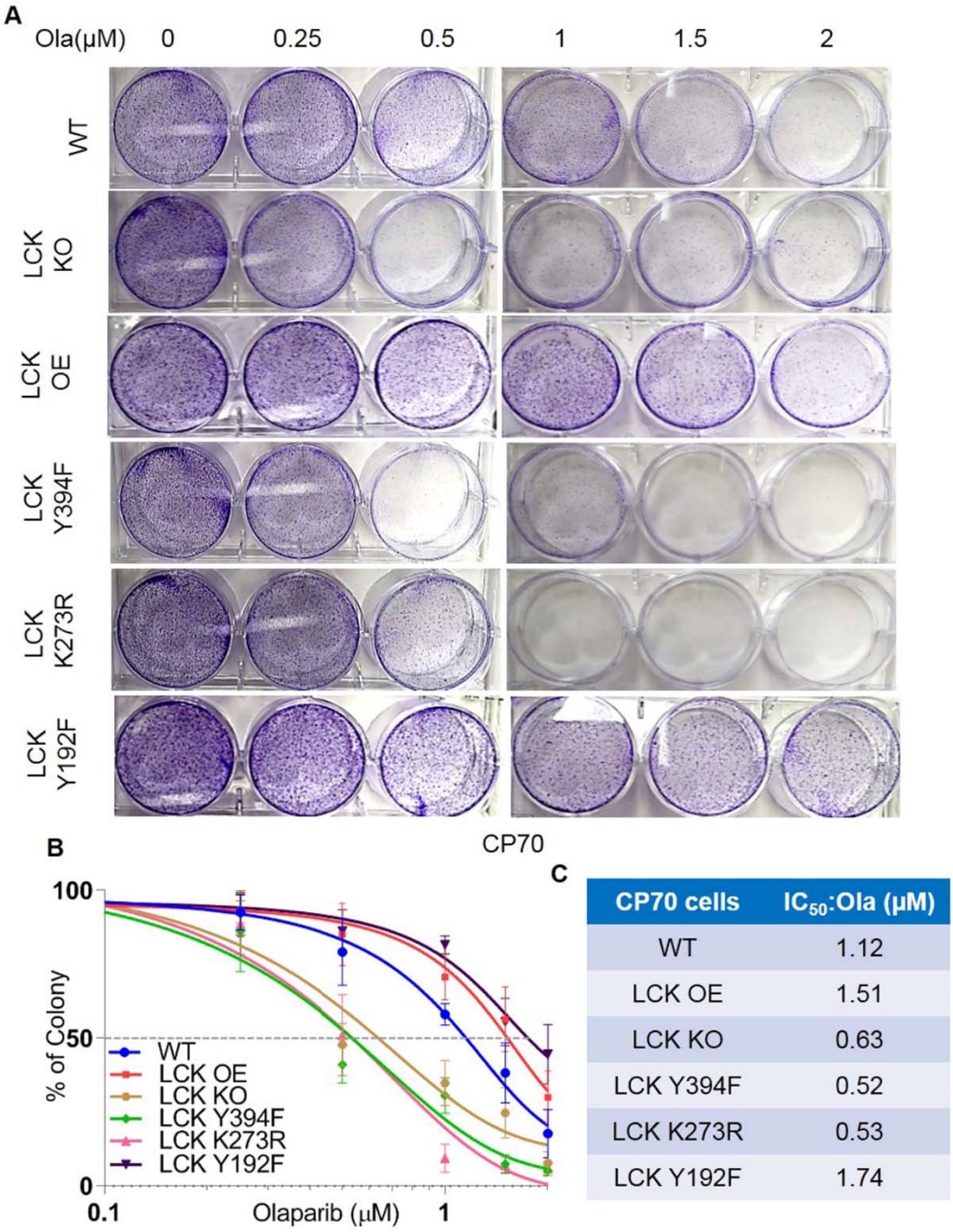

CP70 cells	IC_{50}:Ola (μM)
WT	1.12
LCK OE	1.51
LCK KO	0.63
LCK Y394F	0.52
LCK K273R	0.53
LCK Y192F	1.74

Fig 7: LCK inhibition sensitizes HR-proficient cancer to PARP inhibitor in *in vitro* model. (A) CP70 cells (WT, LCK OE, LCK KO, and LCK Y394F, LCK K273R, and LCK Y192F) were treated with Olaparib in dose dependent manner for 12 days. After that colonies were stained with crystal violet and images were captured. **(B)** Number of Colony formation was counted and plotted as percentage of colony formation in the graph. The IC_{50} values were shown in the table.

Discussion

Approximately 10% of ovarian cancers demonstrate endometrioid tumor (eEOC) histology (2). Advanced ovarian cancers with endometrioid histology are traditionally treated with debulking surgery and cisplatin/taxane-based chemotherapy. Despite high rates of response to initial chemotherapy, many patients recur and become resistant to platinum. eEOC subtype is relatively rare but shows a considerably higher rate of resistance to platinum-based chemotherapy (4) compared to serous carcinomas and do not commonly respond to targeted therapies such as Poly (ADP-Ribose) Polymerase inhibitors (PARPi). Our studies identify a new therapeutic pathway for this subtype of ovarian cancer and identify a strategy for sensitizing HR proficient tumors to PARPi leading to broaden this successful therapy to this eEOC patient population.

We discovered that inhibition of the non-receptor tyrosine kinase LCK attenuates the HR proteins RAD51, BRCA1 and BRCA2 in eEOC. This complements our previous study showing that LCK OE or LCK inhibition with pharmacological inhibitor modulated the mRNA levels of HR DNA repair genes including RAD51, BRCA1, and BRCA2 (15). Here, we show LCK modulates HR genes at the protein level. This has functional consequences as inhibition of LCK via shRNA or pharmacologic inhibitor leads to inhibition in DNA damage as assessed using the established DR-GFP assay in U20S osteosarcoma cells. LCK does not impact NHEJ repairs, an alternate mechanism for repair of double strand breaks by direct ligation independent of an homologous template (27). NHEJ repair proteins Ku70 and Ku80 proteins expression was not impacted by PP2 treatment. We conclude that LCK targets RAD51, BRCA1, and BRCA2 mediated HR repair pathway independent of NHEJ pathway.

We determined for the first time that LCK protein is upregulated in response to DNA damage in eEOC. DNA damage by etoposide, Methyl methanesulfonate (MMS), and UV radiation induces LCK protein expression. This findings is also corroborated with the previous findings that fractionated radiation induced stem cells population displayed LCK activation in human glioma cells (33). In SKOV3 cells as well as UV treated CP70 cells, phosphorylation of LCK (pY394) was elevated in Etoposide, MMS and UV treated cells compared to untreated cells. We found that DNA damage led to nuclear localization of total and pY394 LCK that was further supported by immunofluorescence

analysis of pY394 LCK in response to DNA damage. This finding is unprecedented as LCK is localized on the inner leaflet of the cell membrane at microdomains (34). Previous studies have found constitutively active LCK in the nucleus and binds at the promoter region of LIM domain only 2 (LMO2) leading to gene expression (35). Our findings are significant as we show that LCK is activated by DNA damage leading to nuclear translocation with subsequent activation of HR repair pathways.

Here we show that nuclear translocation of LCK in response to DNA damage leads to coprecipitation with BRCA1 and RAD51. Interaction with BRCA1 and RAD51 requires kinase activity or phosphorylation on Y394, indicating active LCK is necessary for complex formation (29). In contrast, phosphorylation on Y192 is not required for interaction. Moreover, the kinase activity and autophosphorylation is necessary for functional DNA repair based on γH2AX and RAD51 foci formation assay. These findings indicate that LCK kinase activity and autophosphorylation is essential for interaction with HR repair proteins BRCA1 and RAD51 during DNA damage response.

LCK regulates HR repair in response to DNA damage and inhibition potentiates the activity of PARPi to induce synthetic lethality. The simultaneous inhibition of LCK and PARP with pharmacological agents PP2 and Olaparib showed significantly more DNA damage and chromosomal aberration compared to only PP2 or Olaparib treatment in eEOC cells. PP2 treatment was sufficient to attenuate DNA repair that augments the effect of Olaparib in ovarian cancer cells. This provides proof of concept for utility of LCK inhibitors to disrupt HR DNA damage repair. Indeed, several strategies are currently being explored in the clinic to increase use of PARP targeted therapy in HR proficient cancers. CDK1 and CDK12 inhibition led to HR deficiency by decreasing HR repair proteins RAD51, BRCA1, and BRCA2 in lung cancer (11). Further, inhibition of BET proteins also led to attenuation of RAD51 and BRCA1 proteins in breast, ovarian and prostate cancer models (5). PI3K inhibition is also sufficient to reduce BRCA1/2 expression and hampers HR repair in triple negative breast cancer (36). Other reported targets are HSP90 (37) and VEGFR3 (38) to attenuate RAD51, BRCA1 and BRCA2 expressions in ovarian cancer. Concurrent inhibition of PARP enhanced the efficacy of PARPi in above HR proficient cancer models in preclinical settings. Clinical trials are now going on to assess the efficacy of PARPi in combination with CDK1/12 inhibitors,

PI3K inhibitor, and VEGFR3 inhibitors (6). Our findings complement these studies and identify a new signaling pathway for enhancing PARP targeted therapy in eEOC.

In conclusion, these findings provide an innovative new strategy for promoting an HR-deficient status in an otherwise HR-proficient tumor. We identify targeted therapies that compromise HR repair genes to augment sensitivity to PARPi. Our study defines the mechanistic impact of LCK and potentially, nonreceptor tyrosine kinases, in regulation of the HR repair that seem crucial to chemotherapy and PARPi response. The studies highlight new clinical application targeting LCK to expand PARPi utility.

Methods

Cell lines and culture conditions

Cisplatin resistant eEOC cancer cells CP70 were a gift from Analisa Difeo (University of Michigan) and SKOV3 were purchased from American Type Culture Collection (ATCC). Others cell lines used in this study are mentioned in resource table. Cells were grown in DMEM and McCoy's 5A media respectively, supplemented with 10% fetal bovine serum at 37°C in humidified incubator in 5% CO2. Cells were tested and confirmed as mycoplasma contamination negative on a quarterly basis. Cells were passaged by treatment with trypsin/EDTA solution when they reached 80-90% confluence and further passaged or seeded for experiments.

Chemicals and reagents

We used a number of pharmacological agents in our study. The PARP inhibitor (Olaparib) (16), the LCK inhibitor (PP2) (17,18) and the radiomimetic drug, etoposide (19) were purchased as shown in the resource table. Inhibitors were dissolved in 100% DMSO to make stock concentrations and kept at -20°C until use. The details of chemical, reagents, primary antibodies, and secondary antibody details are outlined in the resource table.

Plasmid construct mutants

Myc-tagged LCK containing plasmid was generated using pENTR/D-TOPO cloning kit (Thermo Scientific) according to manufacturer instructions. Briefly, Myc-LCK gene block was purchased from Integrated DNA Technologies (IDT, USA). Myc-LCK was cloned into pENTR/D-TOPO vector. The entry clone was further transferred into a destination vector, pLenti CMV Puro DEST (Addgene). The plasmid was validated by DNA

sequencing (Eurofins). LCK mutants LCKY192F, LCKY394F, LCK273R were generated by site directed mutagenesis. Each mutant was cloned into a lenti viral vector, pLenti CMV Puro DEST (Addgene) for subsequent use.

Lentivirus production

Lentiviral particles for LCK silencing were generated using established lab protocols (15). Briefly HEK293T cells were seeded into 6 well plates. The next day cells were transfected with pRSV-Rev, pMDLg/pRRE, pMD2.G and lentivral vector expressing shRNA for targeting LCK (LCK KD1, TRCN0000426292, LCK KD2, TRCN0000001600, LCK KD3, TRCN0000001598, LCK KD4, TRCN0000001599). Following 24h incubation, transfection media was replaced with fresh DMEM medium. 48h post transfection, lentiviral particle containing media was filtered to remove cell debris and added to CP70 and SKOV3 cells. Fresh media was subsequently added to the HEK-293T transfection plates and incubated for an additional 24 hours followed by filtration and addition to further CP70 and SKOV3 cells. Transduced CP70 and SKOV3 cells were identified using 1.5ug/ml and 2ug/ml puromycin (Thermo Scientific) selection respectively.

Generation of CRISPR/Cas9 KO cells

CP70 cells were used to generate LCK CRISPR/Cas9 knockout cells according to the manufacturer protocol (Santa Cruz Biotechnology). Briefly, cells were transfected with GFP labelled LCK CRISPR/Cas9 plasmid using lipofectamine 3000 (Thermo Scientific) in the presence of antibiotic-free, FBS-enriched, Optimem media. Following transfection, cells were kept in transfection medium for 24h, then replaced with fresh culture media. After an additional 24h, transfected cells were screened for GFP expression using a flow cytometer, and the $GFP^{+/high}$ population was isolated and plated as single cells into a 96 well plate. Cells were grown and expanded in accordance with standard culture techniques as stated above, followed by western blotting for LCK protein expression with anti-LCK antibody (0.5 µg/mL, R & D Systems). Clones with the lowest LCK expression compared to parental cells were considered LCK KO cells.

Western blot analysis

Western blot analysis was performed as reported with modifications as follows (20,21). Briefly, cancer cells were washed with chilled Dulbecco's phosphate buffered saline (PBS) two times at the end of treatment. NP-40 lysis buffer (Invitrogen) was added

dropwise to the plates and placed on ice for 10 minutes. The NP-40 lysis buffer contains 50 mM Tris, pH 7.4, 250 mM NaCl, 5 mM EDTA, 50 mM NaF, 1 mM Na3VO4, 1% Nonidet™ P40 (NP40), 0.02% NaN3 and was supplemented with 1mM PMSF and 2 µg/ml protease cocktail inhibitor (PCI) (Sigma Aldrich). Cells were then collected in a 1.5 mL centrifuge tube by scraping, and incubated on ice for one hour with occasional vortexing. Lysates were centrifuged at 10,000rpm for 10 min at 4°C. Protein concentration was measured of each lysate supernatant by BCA kit analysis (Thermo Scientific). Protein samples were then prepared using 6x Laemmli dye containing BME (β-mercapto ethanol) and boiled for 5-10min. Protein samples were subjected to SDS-PAGE gel electrophoresis using pre-made gradient gels (4-20%, Biorad). Proteins were transferred by wet transfer to a PVDF membrane (Millipore) at 4°C overnight. Membranes were then blocked in 5% BSA in TBST for one hour at room temperature, and subsequently, incubated overnight at 4°C in the following primary antibodies: T-LCK (1:1000 R&D Systems), T-LCK (1:1000 Proteintech), P-LCK 394 (1:1000 R&D Systems), RAD51 (1:1000, Proteintech), BRCA1 (1:500, EMD Millipore), BRCA2 (1:500, EMD Millipore), γH2AX (1:1000 Cell Signaling Technology), GAPDH (1:5000 Proteintech), and β-actin (1:4000 Proteintech). After primary antibody incubation membranes were washed three times with TBST (Tris-buffered saline containing 0.1% tween 20) washing buffer on a platform shaker. Membranes were incubated with HRP-conjugated rabbit (1:25000) or mouse (1:25000) secondary antibodies for one hour at room temperature, followed by three washes with TBST buffer. Chemiluminescence reagent (PerkinElmer) was added to detect immobilized proteins in PVDF membranes utilizing the ChemiDoc imaging system. Densitometry was performed using Image J software.

Nuclear protein isolation and co-immunoprecipitation analysis

CP70 and SKOV3 cells transduced with Myc-tagged LCK were treated with etoposide (10µM) or DMSO for 24h followed by replacement with fresh serum-enriched media for an additional 24h. Cells were collected and washed with cold PBS two times, scraped and centrifuged. Cell pellets were then lysed with cytoplasmic and nuclear extraction buffers according to manufacturer protocols (NE-PER Nuclear and Cytoplasmic Extraction Kit, Thermo Scientific). Protein concentrations of nuclear lysates were

estimated using the BCA method outlined above. For co-immunoprecipitation, nuclear protein lysates were incubated with 3µg anti-Myc antibody (Proteintech) or 3µg control antibody (Cell Signaling Technology) overnight at 4°C with gentle rocking. Pre-cleaned protein A/G agarose beads (Thermo Scientific) were added to the lysates and incubated for 4h at 4°C on a rotating mixer. Beads were then collected by centrifugation and washed three times with chilled NP-40 lysis buffer. 6x Laemmli buffer (Alfa Aesar) containing BME was added and beads were boiled for 5 minutes. Samples were separated on SDS-PAGE and processed for western blot analysis as outlined above. Further, LCK overexpression (LCK OE) SKOV3 (without Myc tagged) cells were treated with etoposide (10µM) for 24h. Then, serum-enriched media was added to replace drug-containing media and kept for another 24h. Then, cells were collected, and nuclear lysates were prepared. Further immunoprecipitation/co-immunoprecipitation was performed after RAD51 pulled down as per above described methods.

Gene conversion assay

Gene coversion assay or DR-GFP assay was performed according to reported methods (22). Human osteosarcoma U2OS cells stably transfected with DR-GFP plasmid and I-SceI endonuclease expression vector pCBASce were kindly provided by Maria Jasin at Memorial Sloan-Kettering Cancer Center. Cells were treated with, PP2 (5, 7, and 10µM) or DMSO vehicle for 48h. Cells were then transfected with I-SceI endonuclease expression vector pCBASce using Lipofectamine 3000. In a separate set of experiments, U2OS cells with DR-GFP integration were transfected with sh Con, LCK KD1 or KD4 for 24h and incubated in serum enriched medium for another 24h. Cells were further transfected with I-SceI plasmid for 24h followed by incubation with serum enriched medium for 24h. Live cells (Live/Dead dye kit, Thermo Scientific) were analyzed with a flow cytometer to estimate the percentage of GFP-positive cells.

RAD51 and γH2AX nuclei staining and analysis

Laser scanning confocal microscopy was performed to detect RAD51 and γH2AX foci in cancer cells. Briefly, ovarian cancer cell, CP70 were grown on coverslips and treated with 10µM etoposide or vehicle for 24h followed by an additional 24h in drug-free media. Coverslips were washed with PBS and fixed with 4% paraformaldehyde (Electron Microscopy Sciences) in PBS. Cells were permeabilized with 0.01% triton-X 100 (Fisher

Scientific) for 5 minutes followed by a wash with chilled PBS and blocked with 3% goat serum (Thermo Scientific) for 1h at room temperature. Cells were incubated with anti-RAD51 (1:250, Abcam) or anti-γH2AX (1:300, Cell Signaling Technology) antibodies overnight at 4°C in a humidified chamber. Next, cover slips were washed 3X with PBS. Alexa fluorescent conjugated secondary antibodies were added to the coverslips and incubated for 1h. Coverslips were washed 3x and mounted with DAPI containing Vectashield (Vector Lab). Images were captured by confocal microscope at 63x magnification in oil emersion (Leica SP8 confocal microscope). RAD51 and γH2AX foci were counted on 20 representative cells by image J software.

Metaphase spread analysis

Metaphase spread analysis was performed on LCKi and PARPi treated cells using established methods (23). Briefly, cells were treated with LCK inhibitor, PP2 (5µM) (Selleck Chemicals) and PARP inhibitor, Olaparib (3µM) (Selleck Chemicals) for 48h. After treatment, cells were harvested. Cells were treated with colcemid (50ng/ml) (Sigma) for 1.5h then washed with PBS and placed in 0.075 mol/L KCl (Sigma) solution for 20min. Subsequently, cells were washed with PBS and fixed in carnoy fixative solution (Methanol: acetic acid 3:1) added dropwise followed by one hour incubation. Cell pellets were collected, and fixative solution was added and incubated at 4°C for 24h. Cell pellets were collected and small amount fixative solution was added and cell suspension was slowly dropped on glass slides and allowed to dry at 37°C. Slides were then stained with Giemsa solution (Sigma Aldrich). Images were captured at 100X magnification with a bright field microscope. Abnormalities in chromosomes were quantified (Chromosomal break, gap, radial formation) by visually counting five nuclei per treatment group.

Single Cell Electrophoresis Assay

Single cell electrophoresis assay or comet assay was performed according to a previously reported method (24). This experiment was performed following the manufacturer's instructions (Trevigen). Briefly, CP70 and SKOV3 eEOC cells were treated with 5µM PP2 and/or 3µM Olaparib for 48h. Comet LMAgarose was melted at 90°C for 10min in a water bath then cooled for 20min to 37°C. Treated cells were detached from plates using trypsin. Serum enriched media was added to neutralize the

trypsin. Cell suspension was washed twice with chilled 1X Ca^{++} and Mg^{++} free PBS, and subsequently suspended at 1 X 10^5 cells/ml in chilled 1X PBS buffer (Free of Ca++ and Mg++). For the alkaline comet assay, the cell suspension was mixed with molten LMAgarose at 37°C. Immediately, 50µL LMAgarose mix was spread on glass microscope slides and incubated at 4°C for 30 min in the dark. Slides were incubated in lysis solution (provided in kit) overnight at 4°C. The next day comet slides were incubated in alkaline unwinding solution at room temperature for 20 min. Agarose gel electrophoresis (21volts for 30min) was performed using alkaline electrophoresis protocol. After electrophoresis, slides were briefly immersed in distilled water twice and then immersed in 70% ethyl alcohol for 5 min. Slides were dried and 100µl of SYBR gold (excitation/emission is 496 nm/522 nm) was added on agarose and kept for 30 min in the dark. Slides were washed with water, dried, and visualized by fluorescence microscopy.

Colony formation assay

The pharmacological effect of Olaparib in cancer cells was investigated by colony formation assay according to the earlier reported method (23). Briefly, ovarian cancer cells CP70 and SKOV3 cells (WT, sh, LCK OE, LCK KO, LCK KD and mutants) were placed on 12 well plates. The next day, cells were treated with Olaparib in a dose dependent manner for 12 days. During this time the media was changed every day using fresh drug. At the end of experiment, PBS was added to the well to wash the colony. Then, cells were fixed with 4% paraformaldehyde solution for 10min. Cells were then washed two times with PBS and incubated in 0.2% crystal violet solution for one hour at room temperature. After incubation cells were washed three times with PBS. Then, the images of six well plates were captured and number of colony forming area was analyzed by Image J software.

Cell titer glo viability assay

CP70 (WT, OE, KD, KO and LCK mutants, Y394F, K273R and Y192F) cells were collected after trypsinization. Cells were counted and 4000 cells were plated in each well of a 96 well plate. Cells were then treated with etoposide for 48h in a dose dependent manner. Control cells were treated with vehicle (DMSO). After the drug treatment, Cell TiterGlo® Luminescent Cell viability assay reagent (Promega) mixture

was prepared and added to the cells to lyse them for 10 minutes shaking and luminescence was measured via luminometer. Cell viability percentage was calculated as luminescence of treated group/luminescence of vehicle treated group×100.

NHEJ gene expression

To check for NHEJ expression, CP70 and SKOV3 cells were grown on 60mm petri dishes until 70% confluent. Cells were then treated with PP2 in a dose dependent manner (5, 7 and 10μM) for 48h and collected by scraping and Western blot was performed to assess protein expression of NHEJ markers Ku70 and Ku80.

Software and Statistics

Graph pad prism software was utilized for graph preparation and to determine statistical significance (detailed in each figure legend). Image J was used for quantification of data. Each experiment was performed at least three times. A p-value less than 0.05 was considered significant.

Acknowledgments

Authors thank the members of Reizes and Lathia Laboratories for helping to improve the scientific quality of the manuscript. We thank Dr. Gauravi Deshpande for helping in image acquisition by confocal microscopy, Amy Graham and Eric Schultz for flow cytometry, and Drs. Debjit Khan and Krishnendu Khan from Fox Laboratory for insights on complex formation assays. We would also like to thank Dr. Suparna Mazumdar (Cleveland Clinic) for giving constructive comments of this study. Research in the Reizes laboratory is funded by Center of Research Excellence in Gynecologic Cancer from the Cleveland Clinic Foundation, VeloSano Bike to Cure, and the Laura J. Fogarty Endowed Chair for Uterine Cancer Research. Dr. Gong is supported by and NIH/NCI grant (R01 CA222195).

References

1. Siegel RL, Miller KD, Jemal A. Cancer statistics, 2020. CA: A Cancer Journal for Clinicians **2020**;70(1):7-30 doi 10.3322/caac.21590.
2. Meinhold-Heerlein I, Fotopoulou C, Harter P, Kurzeder C, Mustea A, Wimberger P*, et al.* The new WHO classification of ovarian, fallopian tube, and primary peritoneal cancer and its clinical implications. Arch Gynecol Obstet **2016**;293(4):695-700 doi 10.1007/s00404-016-4035-8.

3. Winterhoff B, Hamidi H, Wang C, Kalli KR, Fridley BL, Dering J*, et al.* Molecular classification of high grade endometrioid and clear cell ovarian cancer using TCGA gene expression signatures. Gynecol Oncol **2016**;141(1):95-100 doi 10.1016/j.ygyno.2016.02.023.
4. Ren T, Sun TT, Wang S, Sun J, Xiang Y, Shen K*, et al.* Clinical analysis of chemo-resistance risk factors in endometriosis associated ovarian cancer. J Ovarian Res **2018**;11(1):40 doi 10.1186/s13048-018-0418-8.
5. Yang L, Zhang Y, Shan W, Hu Z, Yuan J, Pi J*, et al.* Repression of BET activity sensitizes homologous recombination-proficient cancers to PARP inhibition. Sci Transl Med **2017**;9(400) doi 10.1126/scitranslmed.aal1645.
6. Konstantinopoulos PA, Ceccaldi R, Shapiro GI, D'Andrea AD. Homologous Recombination Deficiency: Exploiting the Fundamental Vulnerability of Ovarian Cancer. Cancer Discov **2015**;5(11):1137-54 doi 10.1158/2159-8290.CD-15-0714.
7. O'Connor MJ. Targeting the DNA Damage Response in Cancer. Mol Cell **2015**;60(4):547-60 doi 10.1016/j.molcel.2015.10.040.
8. Moore K, Colombo N, Scambia G, Kim BG, Oaknin A, Friedlander M*, et al.* Maintenance Olaparib in Patients with Newly Diagnosed Advanced Ovarian Cancer. N Engl J Med **2018**;379(26):2495-505 doi 10.1056/NEJMoa1810858.
9. Galluzzi L, Senovilla L, Vitale I, Michels J, Martins I, Kepp O*, et al.* Molecular mechanisms of cisplatin resistance. Oncogene **2012**;31(15):1869-83 doi 10.1038/onc.2011.384.
10. Tumiati M, Hietanen S, Hynninen J, Pietila E, Farkkila A, Kaipio K*, et al.* A Functional Homologous Recombination Assay Predicts Primary Chemotherapy Response and Long-Term Survival in Ovarian Cancer Patients. Clin Cancer Res **2018**;24(18):4482-93 doi 10.1158/1078-0432.CCR-17-3770.
11. Johnson N, Li YC, Walton ZE, Cheng KA, Li D, Rodig SJ*, et al.* Compromised CDK1 activity sensitizes BRCA-proficient cancers to PARP inhibition. Nat Med **2011**;17(7):875-82 doi 10.1038/nm.2377.
12. Alagpulinsa DA, Ayyadevara S, Yaccoby S, Shmookler Reis RJ. A Cyclin-Dependent Kinase Inhibitor, Dinaciclib, Impairs Homologous Recombination and Sensitizes Multiple Myeloma Cells to PARP Inhibition. Mol Cancer Ther **2016**;15(2):241-50 doi 10.1158/1535-7163.MCT-15-0660.
13. Abbotts R, Topper MJ, Biondi C, Fontaine D, Goswami R, Stojanovic L*, et al.* DNA methyltransferase inhibitors induce a BRCAness phenotype that sensitizes NSCLC to PARP inhibitor and ionizing radiation. Proc Natl Acad Sci U S A **2019**;116(45):22609-18 doi 10.1073/pnas.1903765116.
14. Johnson SF, Cruz C, Greifenberg AK, Dust S, Stover DG, Chi D*, et al.* CDK12 Inhibition Reverses De Novo and Acquired PARP Inhibitor Resistance in BRCA Wild-Type and Mutated Models of Triple-Negative Breast Cancer. Cell Rep **2016**;17(9):2367-81 doi 10.1016/j.celrep.2016.10.077.
15. Saygin C, Wiechert A, Rao VS, Alluri R, Connor E, Thiagarajan PS*, et al.* CD55 regulates self-renewal and cisplatin resistance in endometrioid tumors. J Exp Med **2017**;214(9):2715-32 doi 10.1084/jem.20170438.
16. Yap TA, Kristeleit R, Michalarea V, Pettitt SJ, Lim JSJ, Carreira S*, et al.* Phase I Trial of the PARP Inhibitor Olaparib and AKT Inhibitor Capivasertib in Patients

with BRCA1/2- and Non-BRCA1/2-Mutant Cancers. Cancer Discov **2020**;10(10):1528-43 doi 10.1158/2159-8290.CD-20-0163.

17. Zhu X, Kim JL, Newcomb JR, Rose PE, Stover DR, Toledo LM*, et al.* Structural analysis of the lymphocyte-specific kinase Lck in complex with non-selective and Src family selective kinase inhibitors. Structure **1999**;7(6):651-61 doi 10.1016/s0969-2126(99)80086-0.
18. Nyakeriga AM, Garg H, Joshi A. TCR-induced T cell activation leads to simultaneous phosphorylation at Y505 and Y394 of p56(lck) residues. Cytometry A **2012**;81(9):797-805 doi 10.1002/cyto.a.22070.
19. Best OG, Gardiner AC, Majid A, Walewska R, Austen B, Skowronska A*, et al.* A novel functional assay using etoposide plus nutlin-3a detects and distinguishes between ATM and TP53 mutations in CLL. Leukemia **2008**;22(7):1456-9 doi 10.1038/sj.leu.2405092.
20. Jimenez-Pascual A, Hale JS, Kordowski A, Pugh J, Silver DJ, Bayik D*, et al.* ADAMDEC1 Maintains a Growth Factor Signaling Loop in Cancer Stem Cells. Cancer Discov **2019**;9(11):1574-89 doi 10.1158/2159-8290.CD-18-1308.
21. Bharti R, Dey G, Das AK, Mandal M. Differential expression of IL-6/IL-6R and MAO-A regulates invasion/angiogenesis in breast cancer. Br J Cancer **2018**;118(11):1442-52 doi 10.1038/s41416-018-0078-x.
22. Weinstock DM, Nakanishi K, Helgadottir HR, Jasin M. Assaying double-strand break repair pathway choice in mammalian cells using a targeted endonuclease or the RAG recombinase. Methods Enzymol **2006**;409:524-40 doi 10.1016/S0076-6879(05)09031-2.
23. Kim H, George E, Ragland R, Rafail S, Zhang R, Krepler C*, et al.* Targeting the ATR/CHK1 Axis with PARP Inhibition Results in Tumor Regression in BRCA-Mutant Ovarian Cancer Models. Clin Cancer Res **2017**;23(12):3097-108 doi 10.1158/1078-0432.CCR-16-2273.
24. Pillay N, Tighe A, Nelson L, Littler S, Coulson-Gilmer C, Bah N*, et al.* DNA Replication Vulnerabilities Render Ovarian Cancer Cells Sensitive to Poly(ADP-Ribose) Glycohydrolase Inhibitors. Cancer Cell **2019**;35(3):519-33 e8 doi 10.1016/j.ccell.2019.02.004.
25. Nakanishi K, Cavallo F, Brunet E, Jasin M. Homologous recombination assay for interstrand cross-link repair. Methods Mol Biol **2011**;745:283-91 doi 10.1007/978-1-61779-129-1_16.
26. Scully R, Panday A, Elango R, Willis NA. DNA double-strand break repair-pathway choice in somatic mammalian cells. Nat Rev Mol Cell Biol **2019**;20(11):698-714 doi 10.1038/s41580-019-0152-0.
27. Chang HHY, Pannunzio NR, Adachi N, Lieber MR. Non-homologous DNA end joining and alternative pathways to double-strand break repair. Nat Rev Mol Cell Biol **2017**;18(8):495-506 doi 10.1038/nrm.2017.48.
28. Zhu S, Paydar M, Wang F, Li Y, Wang L, Barrette B*, et al.* Kinesin Kif2C in regulation of DNA double strand break dynamics and repair. Elife **2020**;9 doi 10.7554/eLife.53402.
29. Liaunardy-Jopeace A, Murton BL, Mahesh M, Chin JW, James JR. Encoding optical control in LCK kinase to quantitatively investigate its activity in live cells. Nat Struct Mol Biol **2017**;24(12):1155-63 doi 10.1038/nsmb.3492.

30. Kastle M, Merten C, Hartig R, Kaehne T, Liaunardy-Jopeace A, Woessner NM*, et al.* Tyrosine 192 within the SH2 domain of the Src-protein tyrosine kinase p56(Lck) regulates T-cell activation independently of Lck/CD45 interactions. Cell Commun Signal **2020**;18(1):183 doi 10.1186/s12964-020-00673-z.
31. Xiao M, Guo J, Xie L, Yang C, Gong L, Wang Z*, et al.* Let-7e Suppresses DNA Damage Repair and Sensitizes Ovarian Cancer to Cisplatin through Targeting PARP1. Mol Cancer Res **2020**;18(3):436-47 doi 10.1158/1541-7786.MCR-18-1369.
32. Lloyd RL, Wijnhoven PWG, Ramos-Montoya A, Wilson Z, Illuzzi G, Falenta K*, et al.* Combined PARP and ATR inhibition potentiates genome instability and cell death in ATM-deficient cancer cells. Oncogene **2020**;39(25):4869-83 doi 10.1038/s41388-020-1328-y.
33. Kim RK, Yoon CH, Hyun KH, Lee H, An S, Park MJ*, et al.* Role of lymphocyte-specific protein tyrosine kinase (LCK) in the expansion of glioma-initiating cells by fractionated radiation. Biochem Biophys Res Commun **2010**;402(4):631-6 doi 10.1016/j.bbrc.2010.10.072.
34. Bijlmakers MJ, Marsh M. Trafficking of an acylated cytosolic protein: newly synthesized p56(lck) travels to the plasma membrane via the exocytic pathway. J Cell Biol **1999**;145(3):457-68 doi 10.1083/jcb.145.3.457.
35. Venkitachalam S, Chueh FY, Yu CL. Nuclear localization of lymphocyte-specific protein tyrosine kinase (Lck) and its role in regulating LIM domain only 2 (Lmo2) gene. Biochem Biophys Res Commun **2012**;417(3):1058-62 doi 10.1016/j.bbrc.2011.12.095.
36. Ibrahim YH, Garcia-Garcia C, Serra V, He L, Torres-Lockhart K, Prat A*, et al.* PI3K inhibition impairs BRCA1/2 expression and sensitizes BRCA-proficient triple-negative breast cancer to PARP inhibition. Cancer Discov **2012**;2(11):1036-47 doi 10.1158/2159-8290.CD-11-0348.
37. Choi YE, Battelli C, Watson J, Liu J, Curtis J, Morse AN*, et al.* Sublethal concentrations of 17-AAG suppress homologous recombination DNA repair and enhance sensitivity to carboplatin and olaparib in HR proficient ovarian cancer cells. Oncotarget **2014**;5(9):2678-87 doi 10.18632/oncotarget.1929.
38. Lim JJ, Yang K, Taylor-Harding B, Wiedemeyer WR, Buckanovich RJ. VEGFR3 inhibition chemosensitizes ovarian cancer stemlike cells through down-regulation of BRCA1 and BRCA2. Neoplasia **2014**;16(4):343-53 e1-2 doi 10.1016/j.neo.2014.04.003.

KEY RESOURCES TABLE

REAGENT or RESOURCE	SOURCE	IDENTIFIER
Antibodies		
Anti-LCK antibody	Proteintech	12477-1-AP
Anti-LCK antibody	R&D System	MAB3704
Anti-P-LCK (Y394) antibody	R & D system	MAB7500
Anti-RAD51 antibody	Proteintech	14961-1-AP
Anti-RAD51 antibody	Santa Cruz	sc-398587
Anti-P-H2A.X (Ser139) Antibody	Cell signaling	2577S
Anti-BRCA1 antibody	EMD Millipore	OP-92-100UG
Anti-BRCA2 antibody	EMD Millipore	OP-95-100UG
Anti-Myc antibody	Proteintech	60003-2-Ig
Anti-GAPDH antibody	Proteintech	HRP-60004
Anti-Lamin A/C antibody	Proteintech	10298-1-AP
Alpha Tubulin Monoclonal antibody	Proteintech	HRP-66031
Anti-Ku70 antibody	Proteintech	10723-1-AP
Anti-Ku80 antibody	Proteintech	16389-1-AP
Rabbit IgG XP® Isotype Control	Cell signaling	3900S
Mouse IgG XP® Isotype Control	Cell signaling	5415S
Anti-Rabbit IgG (H+L), HRP antibody	Promega	W4018
Anti-Mouse IgG (H+L), HRP antibody	Promega	W4028
Goat anti-Rabbit IgG Alexa Fluor 488	Thermo	A32731
Goat anti-mouse IgG Alexa Fluor 568	Thermo	A11031

Chemicals and reagents		
Precision Plus Protein™ Kaleidoscope	Biorad	1610375
Olaparib	Selleck chemicals	S1060
PP2	Selleck chemicals	S7008
Etoposide	Selleck chemicals	S1225
Cisplatin	Fesenius Kabi	401572I
Colcemid	Sigma	10295892001
Laemmli SDS sample buffer, reducing (6X)	Alfa Aesar	J61337
Pierce™ Protein A/G Plus Agarose	Thermo	20423
Precision Plus Protein™ Kaleidoscope™	1610375	Biorad
SYBR™ Gold Nucleic Acid Gel Stain	Thermo	S11494
Trypan Blue	Fisher scientific	25900CI
Immobilon-P PVDF Membrane	Merck Millipore	IPVH00010
Critical Commercial Assays		
VECTASHIELD® Mounting Medium	Vector lab	H-1200
NP40 Lysis buffer	Thermo	FNN0021
Pierce™ IP Lysis Buffer	Thermo	87788
Comet Assay Kit	Trevigen	4250-050-K
NuPAGE™ Protein Gel	Thermo	NP0329BOX
4–20% Mini-PROTEAN Protein Gels	Biorad	4568096
Pierce BCA Protein Assay Kit	Thermo	23225
Lipofectamin 3000	Thermo	L3000001
CellTiter-Glo® 2.0 Cell Viability Assay	Promega	G9241
Live/Dead assay kit	Thermo	L23105
KaryoMAX™ Giemsa Stain Solution	Thermo	10092013
Giemsa Stain, Modified Solution	32884-1L	Sigma
NP40 lysis buffer	Invitrogen	FNN0021
Protease Inhibitor Cocktail	Sigma	04693159001
Cytoplasmic and nuclear protein isolation kit	Thermo	78835
Experimental Models: Cell Lines		
CP70	Dr. Analisa Difeo	NA
SKOV3	ATCC	NA
U2OS	Dr. Zihua Gong	NA

U2OS DRGFP reporter cells	Dr. Zihua Gong	NA
HEK293T	ATCC	NA
CRL1978	ATCC	NA
Recombinant DNA		
pLenti CMV Puro DEST	Addgene	NA
Myc-LCK pLenti CMV Puro DEST	In house	
Myc-LCK Y394F pLenti CMV Puro DEST	In house	NA
Myc-LCK K273R pLenti CMV Puro DEST	In house	NA
Myc-LCK Y192F pLenti CMV Puro DEST	In house	NA
I-SceI plasmid	Dr. Zihua Gong	NA
ShRNA targeting LCK	Sigma Aldrich	TRCN0000426292
ShRNA targeting LCK	Sigma Aldrich	TRCN0000001600
ShRNA targeting LCK	Sigma Aldrich	TRCN0000001598
ShRNA targeting LCK	Sigma Aldrich	TRCN0000001599
LCK CRISPR/Cas9 KO Plasmid	Santa Cruz	SC-400434-KO-2
Software		
FlowJo	BD Bioscience	NA
Graph Pad prism	www.graphpad.com	NA
ImageJ	imagej.nih.gov	NA

Supplementary Fig. S1

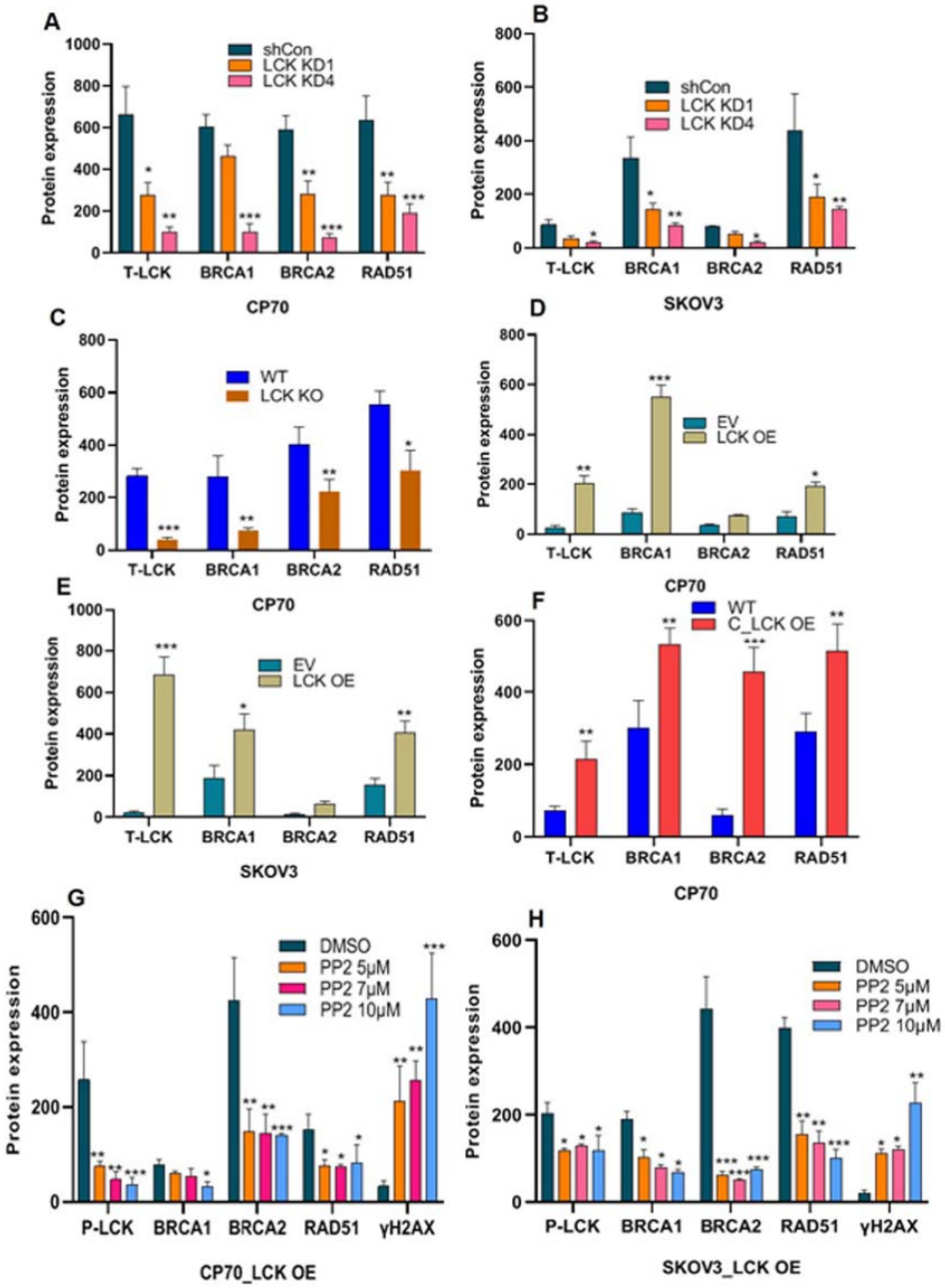

Supplementary Fig. S1: (A) Protein quantification T-LCK, BRCA1, BRCA2 and RAD51 in shCon, LCK KD1, and LCK KD4 CP70 cells as observed in western blot analysis (Main Fig.1A, Left panel). **(B)** Quantification of T-LCK, BRCA1, BRCA2 and RAD51proteins in shCon, LCK KD1, and LCK KD4 SKOV3 cells (Main Fig.1A, second panel from left). **(C)** Quantification of T-LCK, BRCA1, BRCA2, RAD51 protein expression in CP70 WT and LCK KO cells (Main Fig.1A, third panel from left). **(D and E)** Quantification of T-LCK, BRCA1, BRCA2 and RAD51 proteins in CP70 EV and LCK OE (Main Fig.1A, fourth panel from left), and SKOV3 EV and LCK OE cells (Main Fig.1A, fifth panel from left). **(F)** Quantification of T-LCK, BRCA1, BRCA2 and RAD51 proteins in CP70 WT and LCK OE cells in CRISPR/Cas9 background (Main Fig.1A, sixth panel from left). **(G and H)** Protein quantification of P-LCK, BRCA1, BRCA2, RAD51 and

γH2AX in CP70 LCK OE and SKOV3 LCK OE cells treated with PP2 for 48h in a dose dependent manner.

Supplementary Fig. S2

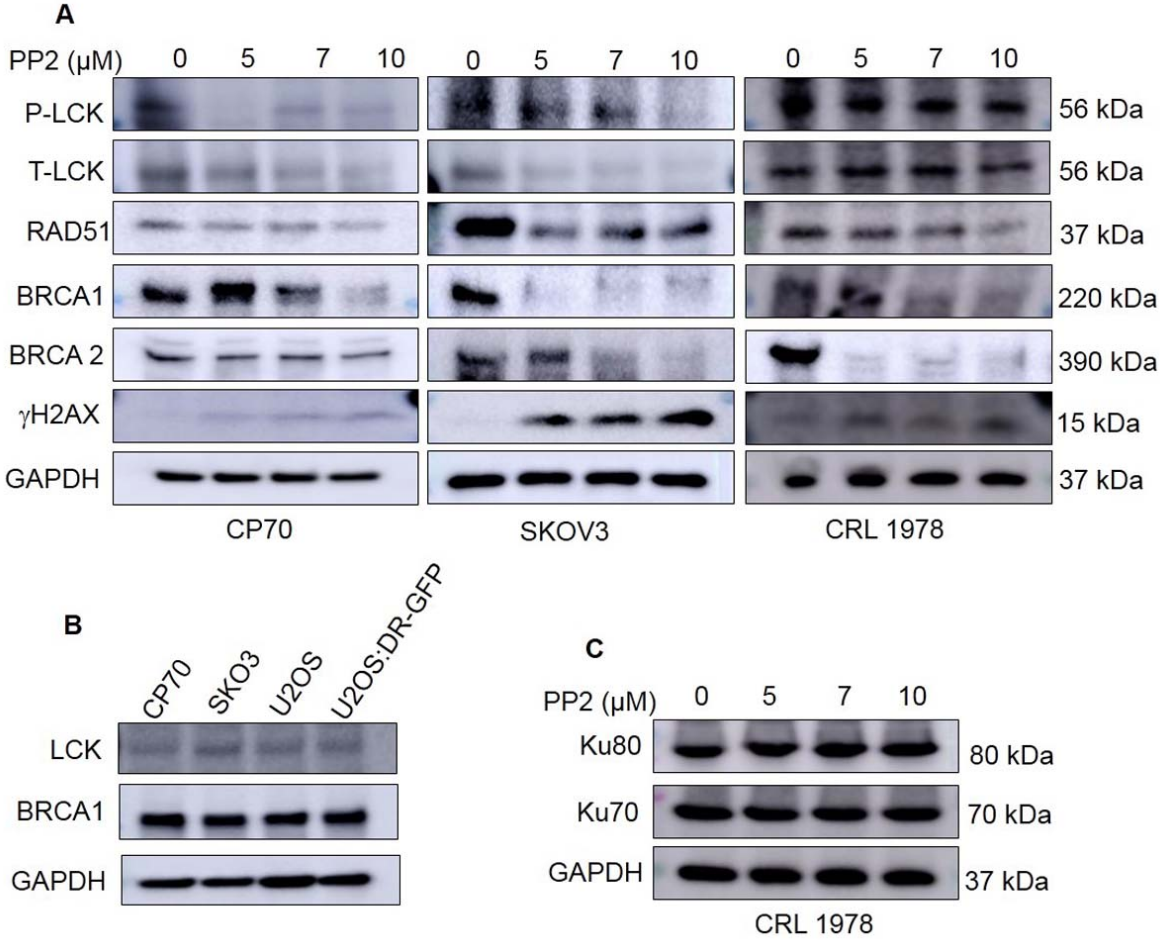

Supplementary Fig. S2: (A) Pharmacological inhibition of LCK attenuates HR repair proteins in ovarian cancer cells. CP70, SKOV3 and CRL1978 cells were treated with the LCKi, PP2 for 48h. Cells were harvested, lysed, and analyzed by immunoblot to assess protein expression of BRCA1, BRCA2, RAD51, and γH2AX. **(B)** Western blot analysis in different cells to check the expression of LCK and BRCA1. U2OS is osteosarcoma cell line which was used in DR GFP assay. U2OS and U2OS: DR-GFP cells were examined for checking LCK and BRCA1 expression. These cells were also found to express LCK and BRCA1 like CP70 and SKOV3 cells. **(C)** CRL1978 cells were treated with increasing concentrations of PP2 for 48h and cells were harvested, lysed, and immunoblotted for Ku70, and Ku80 protein expression. GAPDH was used as loading control.

Supplementary Fig. S3

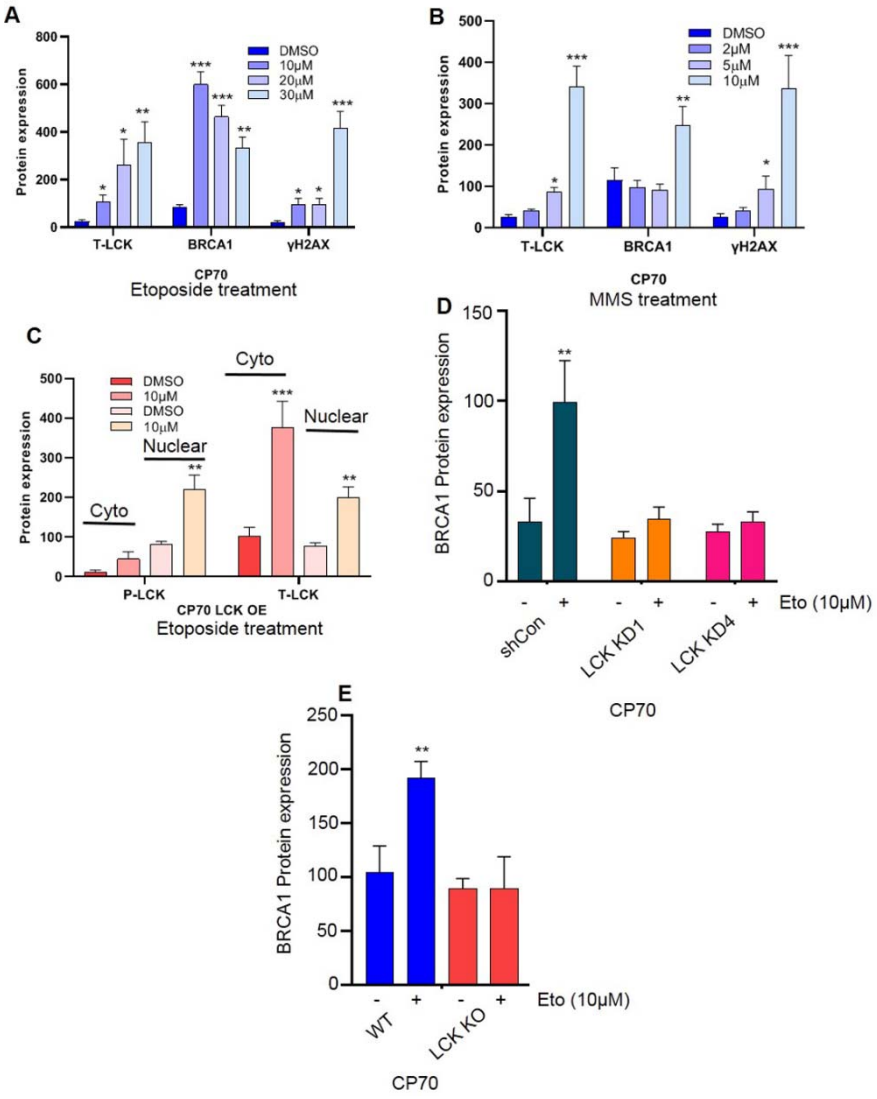

Supplementary Fig. S3 (A, B) Protein quantification of T-LCK, BRCA1, and γH2AX in CP70 cells treated with etoposide and MMS (Main Fig. 2A). **(C)** Quantification of P-LCK and T-LCK in CP70 LCK OE cells treated with etoposide (Main Fig. 2B). **(D)** Quantification of BRCA1 protein in CP70 shCon, LCK KD1 and LCK KD4 cells treated with/without etoposide (Main Fig. 2D). (E) Quantification of BRCA1 protein expression in CP70 WT and LCK KO cells treated with/without etoposide (Main Fig. 2E).

Supplementary Fig. S4

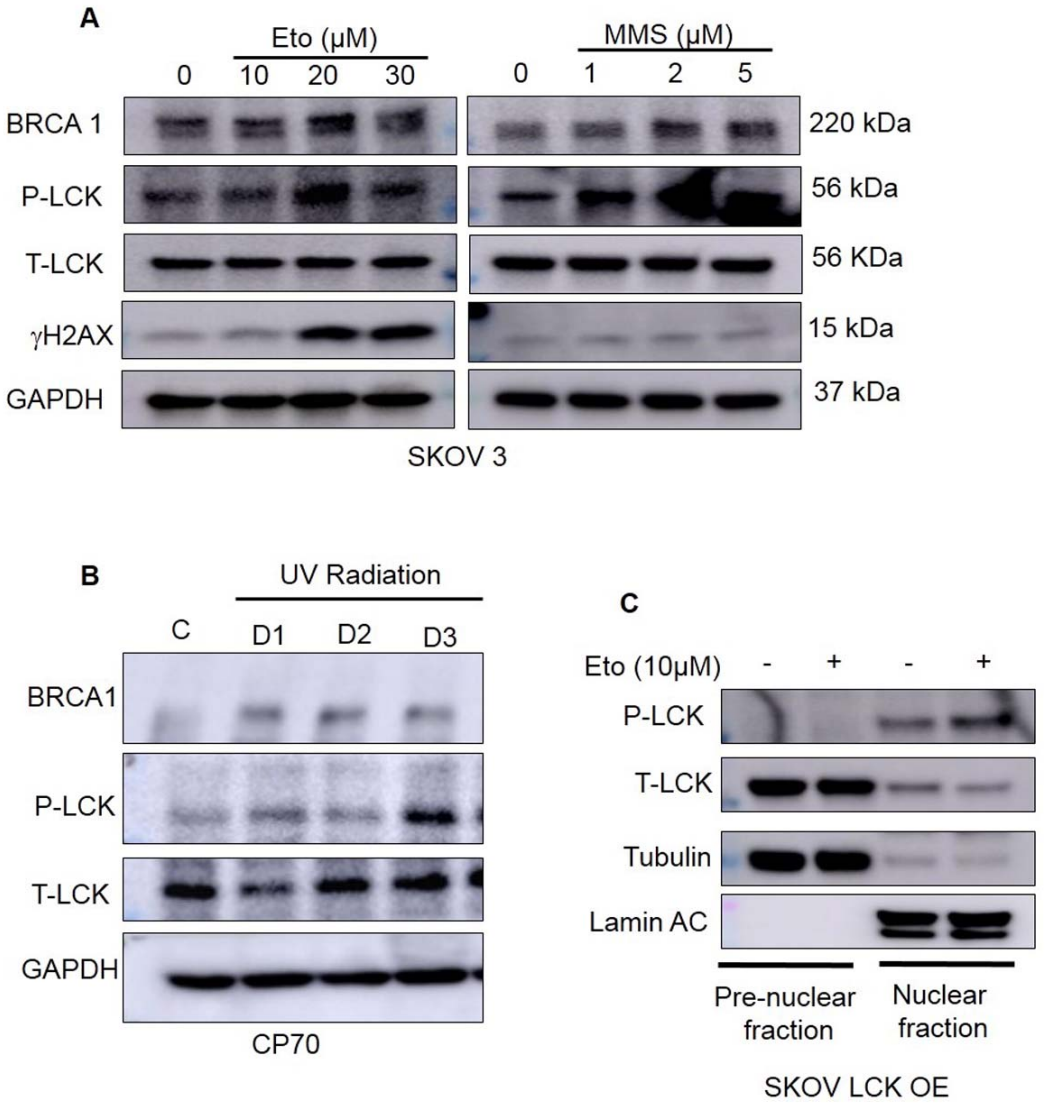

Supplementary Fig. S4: **(A)** SKOV3 cells were treated with etoposide, and MMS for 24. After that cells were put in 24h in drug free media. Cells were then subjected to western blot analysis for checking protein expression. **(B)** DNA damage by UV radiation upregulates LCK phosphorylation. CP70 cells were treated with UV radiation for 1min, 2min and 4min. Cells were kept in serum enriched media for 24h. Then cells were subjected to western blot analysis to check the expression of P-LCK, T-LCK and BRCA1 expression. **(C)** SKOV3 LCK OE cells were treated with etoposide for 24h. Cells were then put in drug free media for another 24h. Cells were collected, and cytoplasmic and nuclear proteins were extracted for western blot analysis.

Supplementary Fig. S5

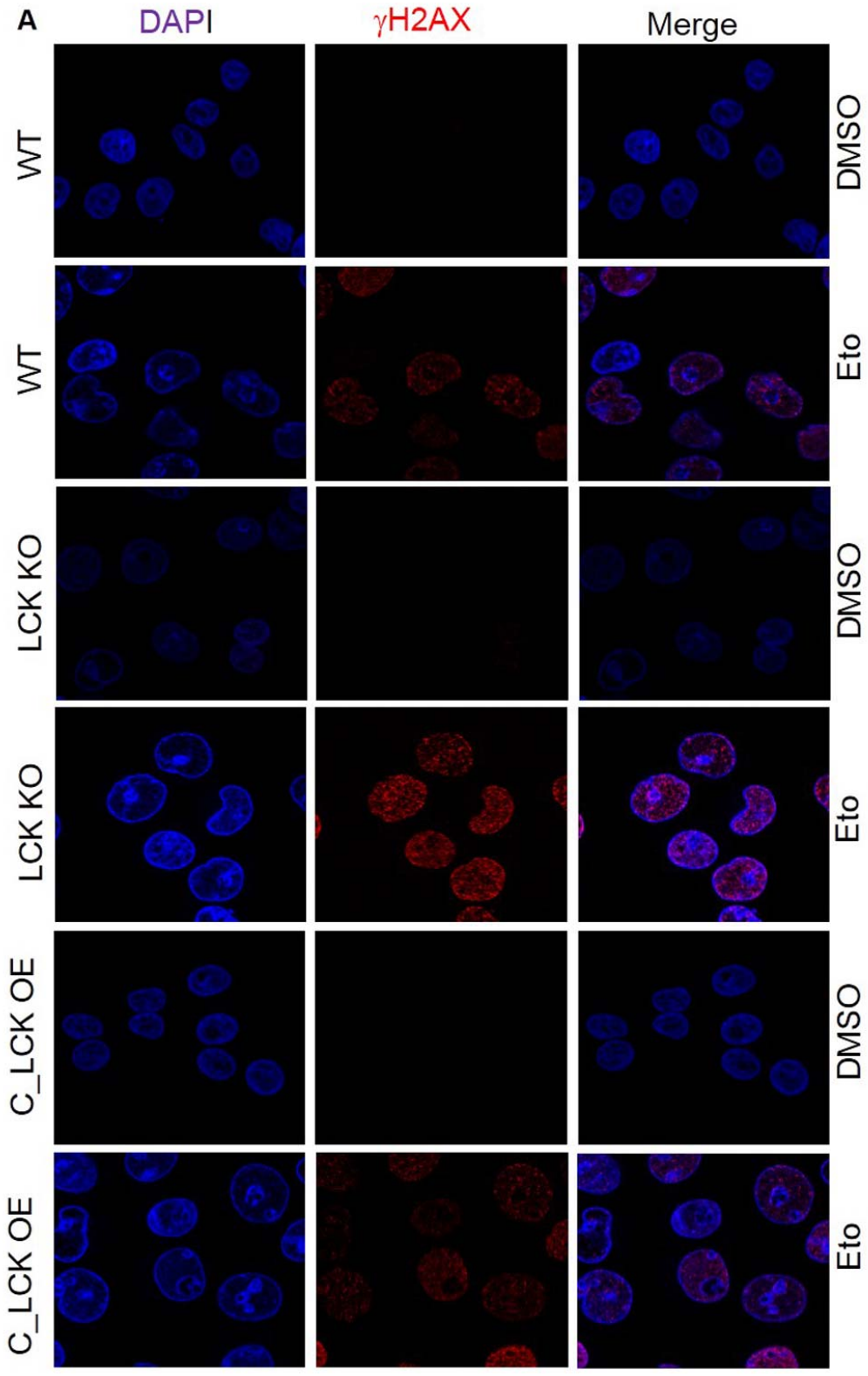

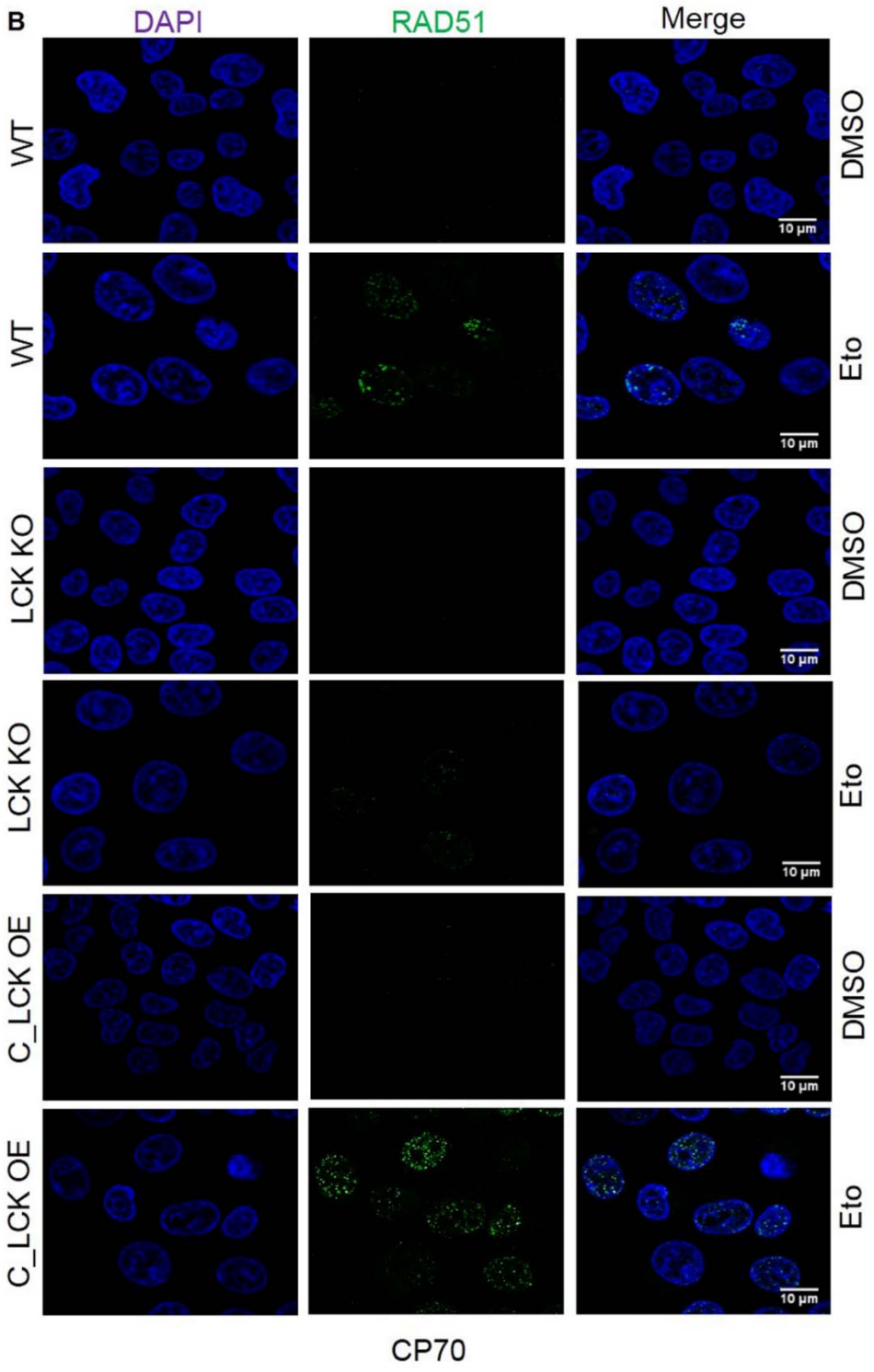

Supplementary Fig. S5 (A) CP70 WT, LCK KO (CRISPR/Cas9) and LCK OE (In CRISPR background) cells were treated with DMSO/etoposide 10µM for 24h. Then cells were kept in drug free media for another 24h. Then immunofluorescence study was performed to visualize γH2AX foci formation in different groups. **(B)** CP70 WT, LCK KO (CRISPR/Cas9) and LCK OE (In CRISPR background) cells were treated with DMSO/etoposide 10µM for 24h. Cells were put in drug free media for another 24h. Then immunofluorescence study was performed to visualize RAD51 foci formation in different groups.

Supplementary Fig. S6

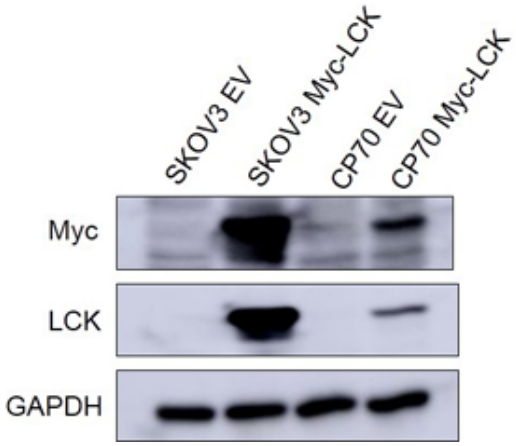

Supplementary Fig. S6: Transfection efficiency of Myc tagged LCK in SKOV3 and CP70. SKOV3 and CP70 cells were transduced with EV or Myc tagged LCK plasmid by using lentiviral particle. Then, cells were checked for Myc and LCK expression.

Supplementary Fig. S7

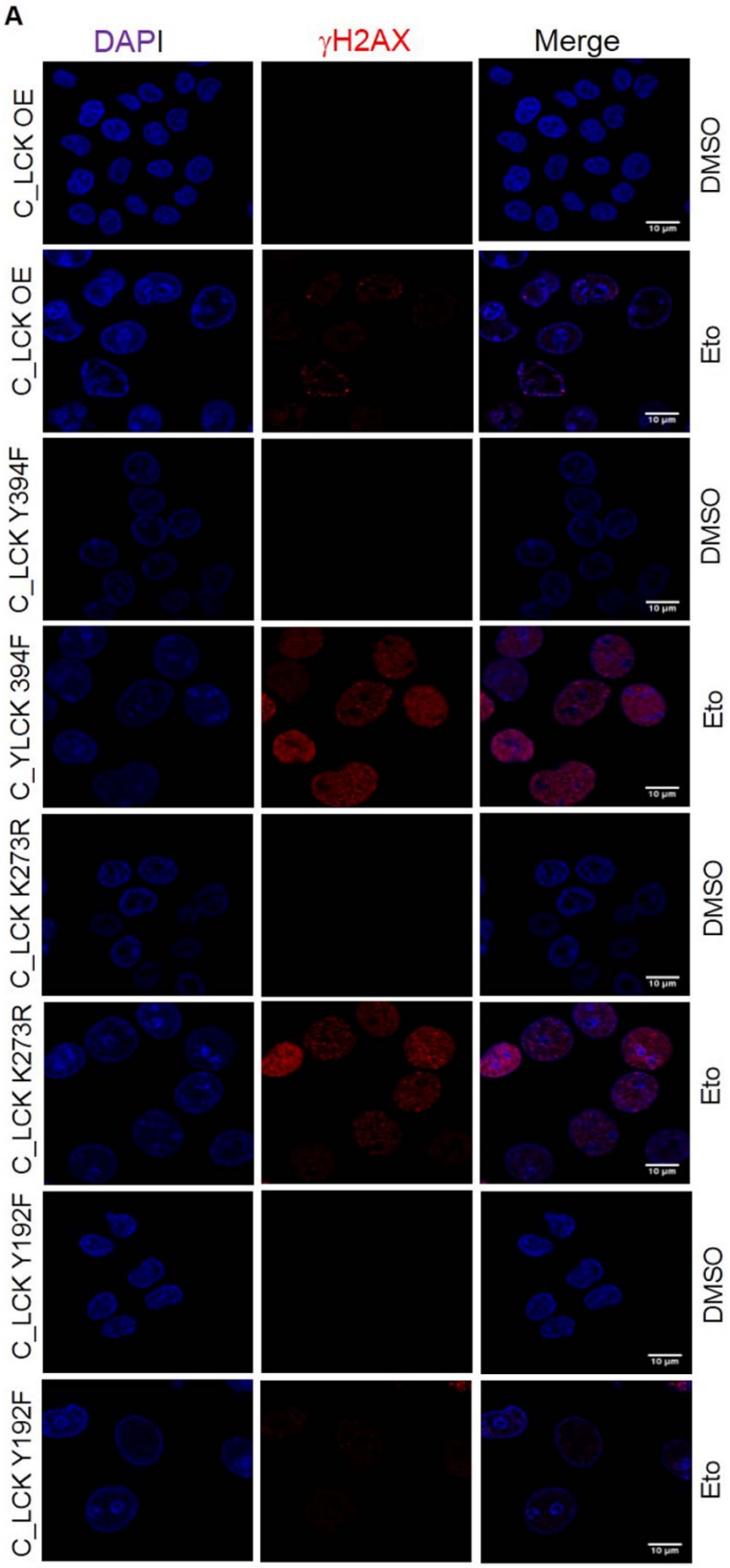

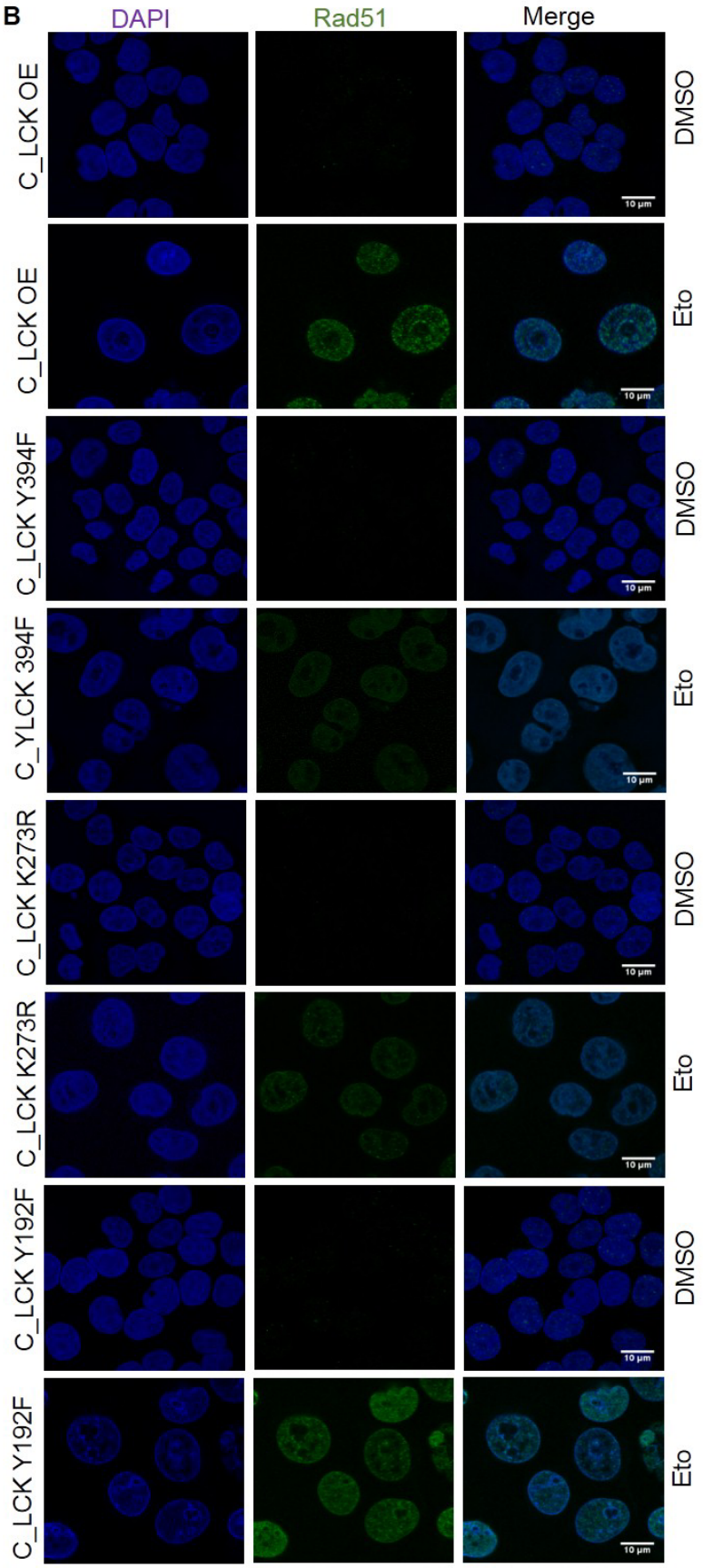

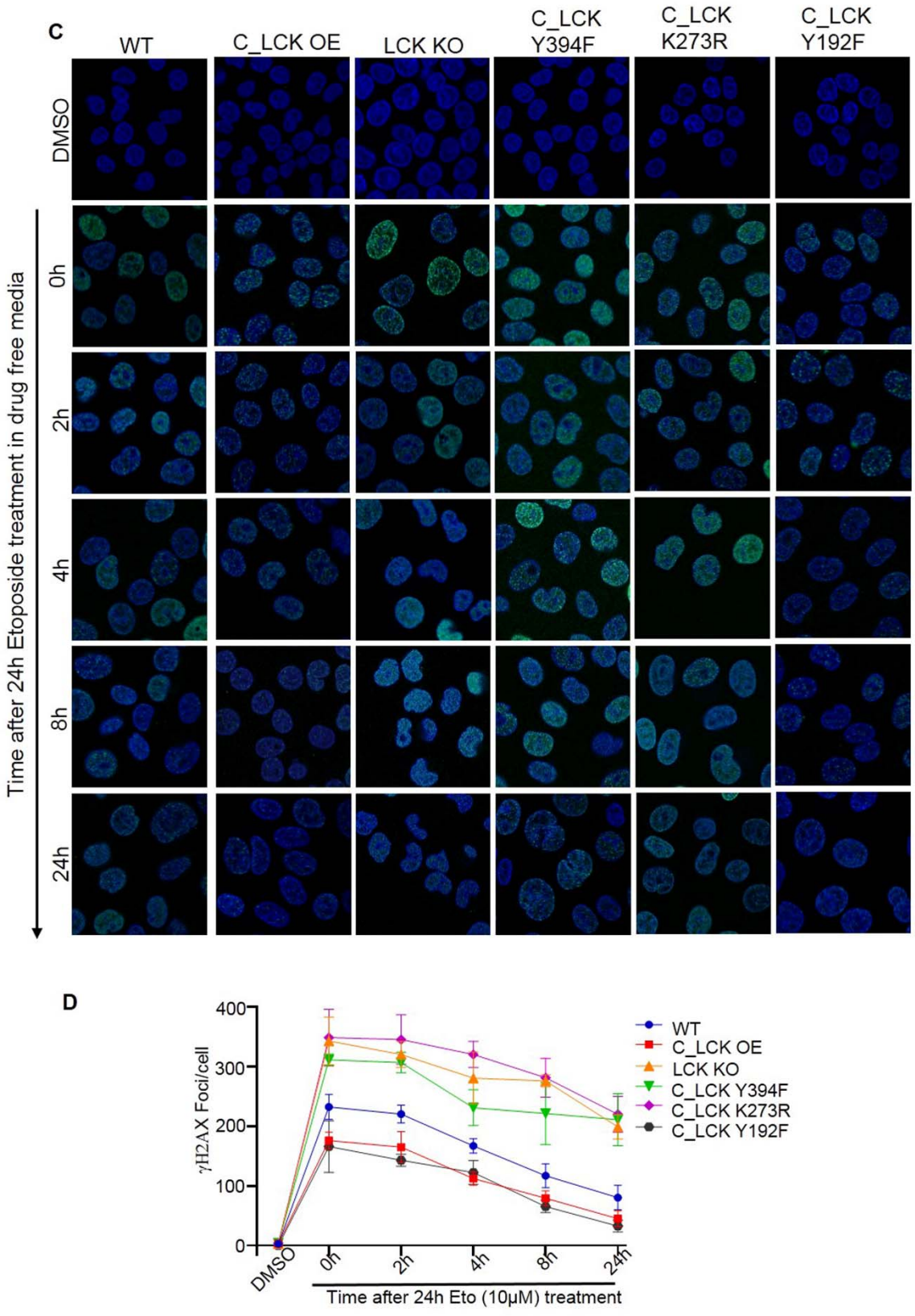

Supplementary Fig. S7: (A) CP70 cells (LCK OE, LCK Y394F, LCK K273R, and LCK Y192F) were treated with etoposide for 24h**.** Cells were then kept in drug free media for 24h. Immunofluorescence study was performed to visualize γH2AX foci formation. **(B)** CP70 cells (LCK OE, LCK Y394F, LCK K273R, and LCK Y192F) were treated with etoposide for 24h**.** Cells were then kept in drug free media for 24h. Immunofluorescence study was performed to visualize RAD51 foci formation. **(C)** γH2AX kinetic study. CP70 cells (WT, LCK OE, LCK KO, LCK Y394F, LCK K273R, and LCK Y192F) were treated with etoposide for 24h. After that cover slips were incubated in drug free media for 0h, 2h, 4h, 8h and 24h. Cover slips were processed for immunofluorescence study to visualize γH2AX foci formation. **(D)**The quantification of foci was performed and plotted in the graph.

Supplementary Fig. S8

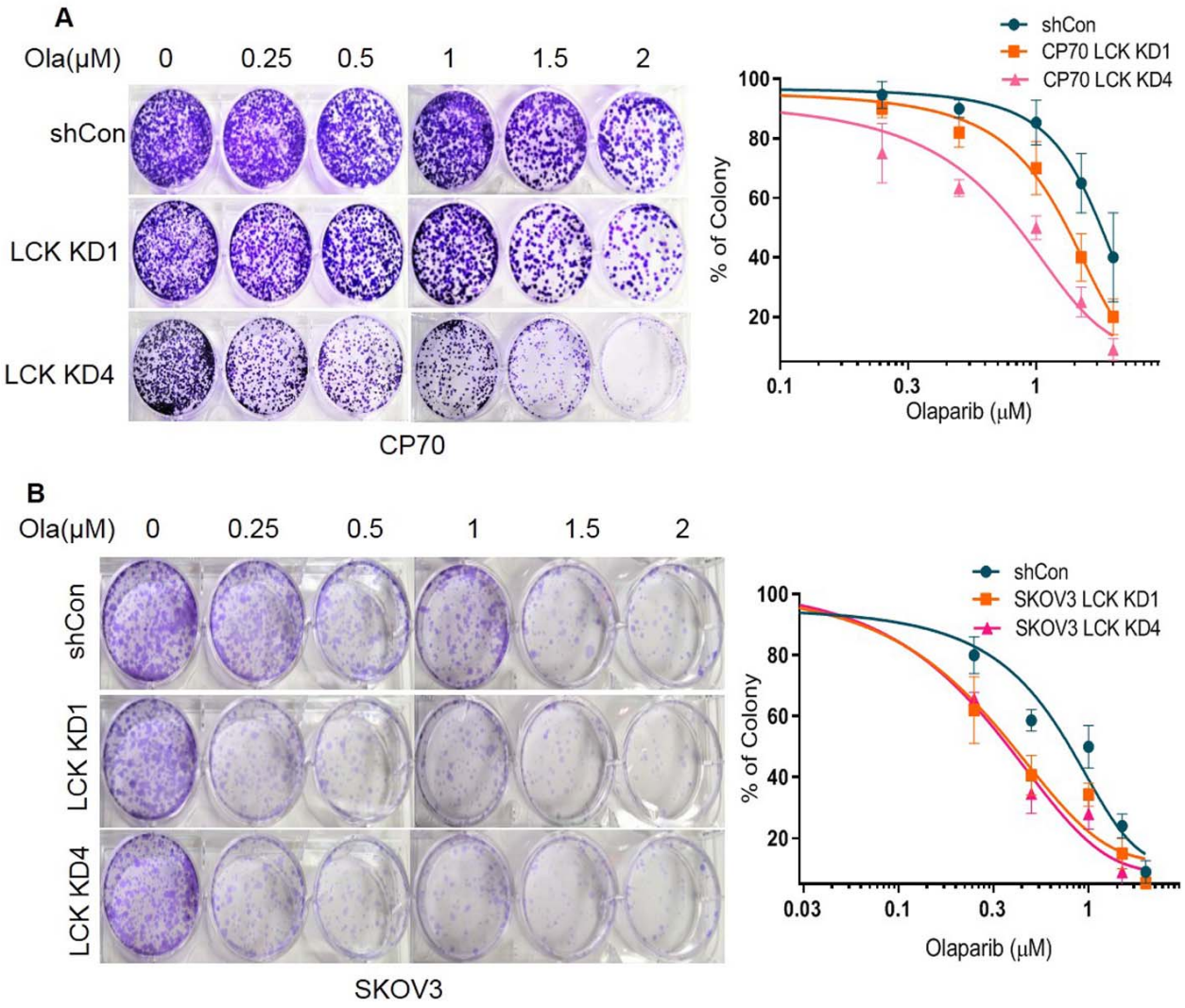

Supplementary Fig. S8: (A) CP70 Sh Con or LCK knock down cells were treated with Olaparib in a dose dependent manner for 12 days. Number of colonies was counted and plotted using graph pad prism. **(B)** SKOV3 Sh Con or LCK knock down cells were treated with Olaparib in dose dependent manner for 12 days. Number of Colony formation was counted and plotted in the graph.